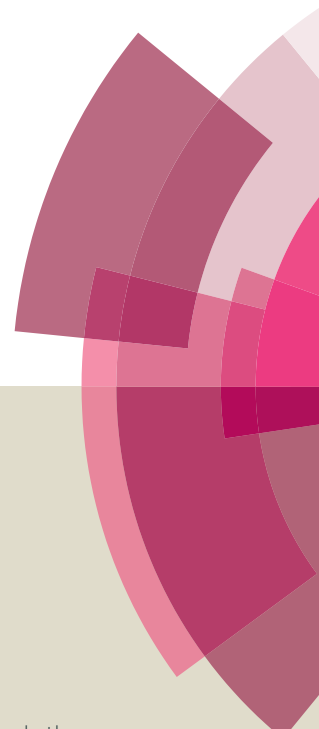
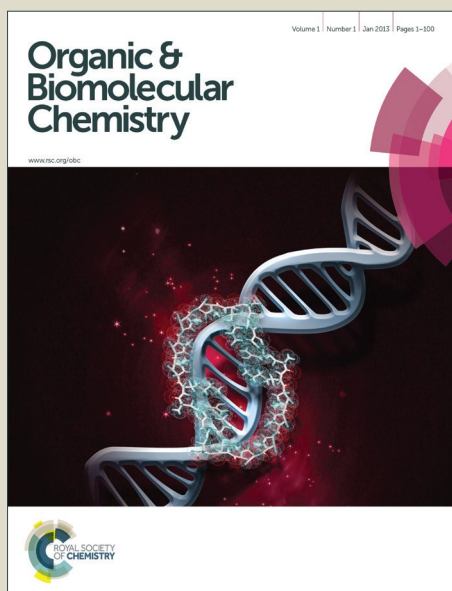


Organic & Biomolecular Chemistry

Accepted Manuscript



This article can be cited before page numbers have been issued, to do this please use: L. Yue, J. Du, F. Ye, Z. Chen, L. Li, F. Lian, B. Zhang, Y. Zhang, H. Jiang, K. Chen, Y. Li, B. Zhou, Y. Yang and C. Luo, *Org. Biomol. Chem.*, 2016, DOI: 10.1039/C6OB01248E.



This is an *Accepted Manuscript*, which has been through the Royal Society of Chemistry peer review process and has been accepted for publication.

Accepted Manuscripts are published online shortly after acceptance, before technical editing, formatting and proof reading. Using this free service, authors can make their results available to the community, in citable form, before we publish the edited article. We will replace this *Accepted Manuscript* with the edited and formatted *Advance Article* as soon as it is available.

You can find more information about *Accepted Manuscripts* in the [Information for Authors](#).

Please note that technical editing may introduce minor changes to the text and/or graphics, which may alter content. The journal's standard [Terms & Conditions](#) and the [Ethical guidelines](#) still apply. In no event shall the Royal Society of Chemistry be held responsible for any errors or omissions in this *Accepted Manuscript* or any consequences arising from the use of any information it contains.

Identification of novel small-molecule inhibitors targeting menin-MLL interaction, repurposing the antidiarrheals loperamide†

Liyan Yue,^{‡a,b} Juanjuan Du,^{‡c} Fei Ye,^{‡d} Zhifeng Chen,^e Lianchun Li,^f Fulin Lian,^{a,b} Bidong Zhang,^{a,b} Yuanyuan Zhang,^{a,b,*} Hualiang Jiang,^{a,b} Kaixian Chen,^{a,e} Yuanchao Li,^c Bing Zhou,^c Yaxi Yang,^{c,*} and Cheng Luo^{a,e,*}

Received 00th January 20xx,
Accepted 00th January 20xx

DOI: 10.1039/x0xx00000x

www.rsc.org/

Leukemia with mixed lineage leukemia (MLL) rearrangement, which harbors a variety of MLL fusion proteins, has a poor prognosis despite the latest improved treatment options. Menin has been reported to be a required cofactor for the leukemogenic activity of MLL fusion proteins. Thus, the disruption of the protein-protein interactions between menin and MLL represents a very promising strategy for curing MLL leukemia. Making use of menin-MLL inhibitors with a shape-based scaffold hopping approach, we have discovered that the antidiarrheals loperamide displays, previously unreported, mild inhibition for the menin-MLL interaction ($IC_{50} = 69 \pm 3 \mu\text{M}$). In an effort to repurpose this drug, a series of chemical modification analysis were performed. And three of the loperamide-based analogues, **DC_YM21**, **DC_YM25** and **DC_YM26** displayed better activities with IC_{50} of $0.83 \pm 0.13 \mu\text{M}$, $0.69 \pm 0.07 \mu\text{M}$ and $0.66 \pm 0.05 \mu\text{M}$ respectively. Further treatment with **DC_YM21** demonstrated potent and selective blockage of proliferation and induction of both cell cycle arrest and differentiation of leukemia cells harboring MLL translocations, which confirmed specific mechanism of action. In conclusion, molecules of a novel scaffold targeting menin-MLL interactions were reported and they may serve as new potential therapeutic agents for MLL leukemia.



Introduction

Dysregulation in epigenetic modifications is closely related to human cancers¹⁻⁵. During the last decade, huge efforts have been put into drug discovery and development of epigenetic targets⁶⁻¹⁰, especially DNA methyltransferase¹¹⁻¹⁴ and histone methyltransferase (HMT)¹⁵⁻¹⁷. Histone modifications play

fundamental roles in many biological processes¹⁸⁻²¹, and aberrances in these “epigenetic modifications” are closely related with the development of human cancers²¹⁻²⁴. The Mixed lineage leukemia 1 (also known as histone-lysine N-methyltransferase 2A, Trithorax-like protein, Zinc finger protein HRX, CXXC-type zinc finger protein 7, ALL-1, KMT2A and MLL1) is a specific H3K4 methyltransferase and it is the subunit of the COMPASS (Complex Proteins Associated with Set1²⁵)-like multi-subunit (SET1/MLL) complex. MLL1 gene encodes a 3,969 amino acid, 500 kDa protein with multiple domains, of which the SET domain that functions as histone methyltransferase is C-terminal located. After being cleaved by Taspse1, the active form MLL^{N320/C180} consisting of N-terminal 320 kDa (MLL^{N320}) and C-terminal 180 kDa (MLL^{C180}) is generated²⁶, and the two fragments remain non-covalently bound in a tight complex in the MLL1 complex. MLL1 protein interacts with WDR5, RBBP5, ASH2L, and Dpy30 through this C-

^a State Key Laboratory of Drug Research, Shanghai Institute of Materia Medica, Chinese Academy of Sciences, Shanghai 201203, China.

^b University of Chinese Academy of Sciences, No.19A Yuquan Road, Beijing 100049, China

^c Department of Medicinal Chemistry, Shanghai Institute of Materia Medica, Chinese Academy of Sciences, Shanghai 201203, China.

^d Zhejiang Sci-Tech University, College of Life Sciences, Hangzhou, China.

^e School of Life Science and Technology, Shanghai Tech University, Shanghai 200031, China.

^f Guangxi Key Laboratory of Functional Phytochemicals Research and Utilization, Guangxi Institute of Botany, Guangxi Zhuang Autonomous Region and Chinese Academy of Sciences, Guilin 541006, China.

†Electronic Supplementary Information (ESI) available. See DOI: 10.1039/x0xx00000x

terminal fragment^{27, 28}, playing an essential role in early development and hematopoiesis. Rearrangement of MLL1 gene at chromosome locus 11q23 occurs frequently in patients with *de novo* acute myeloid (AML) and acute lymphoblastic (ALL) leukemia, and has a poor prognosis with only a ~35% overall 5-year survival rate despite improved treatment options like allogeneic hematopoietic stem cell transplantation^{28, 29}. The rearrangement enables MLL1 protein to fuse its N-terminus to one of partners to yield a collection of chimeric fusion proteins. These fusion proteins showed abnormal functions, upregulating expression of genes such as *HOXA9* and *MEIS1*, resulting in enhanced proliferation and blockage of hematopoietic differentiation^{30, 31}. Over 100 translocations have been reported and more than 70 different partner proteins have been identified³². Among these partners, MLL1 is predominantly fused to nine of them, AF4 (accounts for translocations (t4;11), AF9 (t9;11), ENL (t11;19), AF10 (t10;11), AF6 (t6;11), ELL (t11;19), AF1P, AF17, and SEPT6, accounting for almost 90% of MLL rearrangements²⁹. The fusion partners are often believed to convert the truncated MLL to a potent transcriptional activator^{26, 33-35}.

Menin is a 610 amino acid, 67 kDa protein encoded by the multiple endocrine neoplasia 1 (Men1) gene³⁶. It functions as a tumor suppressor in the similarly-named familial syndrome, an inherited disorder that causes tumors in the endocrine glands and the duodenum³⁷. Menin binds directly to the N-terminus of WT MLL1/2 and all MLL1 fusion proteins. It simultaneously interacts with the N-terminus of MLL and the IBD domain of the chromatin associated protein LEDGF (lens epithelium derived growth factor). As a component of both MLL1 and MLL2 complex, LEDGF is essential for co-localization of menin and wild type MLL or MLL fusions to target genes^{38, 39}. In this way, menin acts as a co-factor in leukemic transformation. Several studies have demonstrated that menin is required for the normal expression of MLL target genes^{40, 41}. A great deal of effort has been put into biochemical and structural studies of identifying the menin-MLL interaction motif^{32, 39, 42-44}. Two short motifs in the N-terminus of MLL with high binding affinity to menin have been identified⁴⁵. The menin binding motif 1 (MBM1) encompasses MLL residues 4-15, binding to menin with high affinity (Kd = 53 nM). The menin binding motif 2 (MBM2) involves residues 23-40, presenting a lower affinity (Kd = 1.4 μM)⁴⁵. Efficient proliferation of myeloid cells transformed with oncogenic MLL-AF9 depends on the existence of menin and loss of menin relieved the differentiation block of MLL-transformed leukemic blasts. Mutations within the N-terminus of MLL fusion proteins that block association with menin showed no activity in inducing leukemia in contrast to the intact protein. Additionally, expression of MLL amino terminal peptides, which can disrupt MLL-menin interaction, results in reduction of menin binding with endogenous MLL as well as growth inhibition of MLL-AF9 transformed cells^{46, 47}. These findings demonstrate that MLL

fusion proteins are dependent on the interaction with menin for their oncogenic activity⁴², and imply that the menin-MLL interaction represents an attractive target for molecular therapy.

Although the interaction between menin and the wild-type MLL protein is reported to be indispensable for *Hox* genes expression in early hematopoietic progenitors to maintain self-renewal abilities⁴⁸, recent studies demonstrate that menin is not a requisite cofactor for MLL1 during normal hematopoiesis and drugs that target menin-MLL1 is safe and selective for MLL-rearranged leukemia^{49, 50}. Using a competition-based fluorescence polarization assay with the fluorescein-labelled MBM1 peptide and menin protein, Grembecka and Cierpicki discovered the first-generation of small-molecule menin-MLL interaction inhibitors, which belong to the thienopyrimidine class⁴³. The optimized **MI-2** inhibits the menin-MBM1 interaction with IC₅₀ = 446 nM⁴³. A more potent analog **MI-2-2** (IC₅₀ = 46 nM) was obtained after structural studies and further medicinal chemistry optimizations, which fits into the central cavity on menin in the MBM1 pocket by mimicking the key interactions of the peptide with menin⁴⁴. Based on **MI-2-2**, **MI-463** (IC₅₀ = 15.3 nM) and **MI-503** (IC₅₀ = 14.7 nM) were recently developed to be two lead inhibitors and have favorable drug-like properties⁴⁸. Furthermore, chemical optimization for better activities and drug-like properties have been thoroughly discussed recently^{51, 52}, with **MI-538** (IC₅₀ = 21±1.4 nM) to be the most potent inhibitor for *in vitro* studies^{51, 52}. The second class of menin-MLL interaction inhibitors are based on the hydroxylmethylpiperidine scaffold. The HTS hit, **MLS001171971** showed an activity of IC₅₀ = 5.8 μM, while modified compounds **ML227** and **ML399** (Molecular Libraries Probe Production Centers Network) displayed better activities with IC₅₀ values of 883 nM and 90 nM respectively²⁸. A similar compound of hydroxyl and aminomethylpiperidine structure was found in the same library, and medicinal chemistry optimization led to compound **MIV-6R** (IC₅₀ = 56 nM), which demonstrated strong and selective effects in MLL leukemia cells⁵³, representing the most potent inhibitor of this class. Recently, two amino-glycoside antibiotics were reported to target the menin-MLL interface⁵⁴. In addition, peptidomimetics **MCP-1** strongly binds to menin with the K_i value of 4.7 nM by mimicking MBM1⁵⁵.

Virtual screening methods including scaffold hopping, docking and pharmacophore as well as other computational methods have been proved to be useful and efficient approaches for novel drug discovery^{12, 14, 16, 56-63}. Based on the hypothesis that compounds sharing high structural similarities may exhibit similar bioactivities⁶⁴, shape-based three-dimensional structure superposition has been proved to be a powerful tool for computational scaffold hopping, providing a desirable approach for discovering novel compounds in a number of cases of ligand-based virtual screening^{65, 66}. In this study, scaffold hopping calculations were conducted making use of

the complex crystal structures of human menin with bound inhibitor **MI-2-2** and **MIV-6R** respectively (PDB ID: 4GQ4 and 4OG8) utilizing SHAFTS^{67, 68}. Considering the drug-like properties of candidates, an in-house library comprising ~1600 compounds was built for 3D similarity searching based on the existing drugs. As a result, loperamide, an antidiarrheal drug used in acute and chronic diarrhea as well as in ileostomy, was identified to inhibit the menin-MLL interaction. Although loperamide showed mild inhibition to menin-MBM1 complex ($IC_{50} = 69 \pm 3 \mu\text{M}$), chemical optimizations led to three improved molecules **DC_YM21**, **DC_YM25** and **DC_YM26** with IC_{50} values of $0.83 \pm 0.13 \mu\text{M}$, $0.69 \pm 0.07 \mu\text{M}$ and $0.66 \pm 0.05 \mu\text{M}$ respectively. These compounds displayed inhibitory activities against menin-MLL in fluorescence polarization assays and cell viability assays like the reported inhibitor **MI-2-2** (**Supplementary information**). Some biophysical experiments including differential scanning fluorimetry (DSF), surface plasmon resonance (SPR) and competition saturation transferred difference (STD) were performed to validate the specific binding of inhibitors to menin at the MBM1 binding site. The results demonstrated that the molecules we obtained from loperamide scaffold can disrupt the menin-MLL interaction both *in vitro* and *in vivo*. Further treatment with **DC_YM21** caused growth inhibition, cell cycle arrest, differentiation induction and down-regulation of MLL fusion target genes expression, representing the specific action of menin-MLL inhibitors. Structure-activity relationship of a series of inhibitors was also discussed, providing some clues for further menin-MLL inhibitor design and development. In short, molecules of a novel scaffold targeting menin-MLL interactions were reported and they may serve as new potential therapeutic agents for MLL leukemia.

Results and discussion

Identifying Loperamide as a Mild menin-MLL Interface Inhibitor

Since **MI-2-2** and **MIV-6R** are representative compounds of two classes of menin-MLL inhibitors, they were used to query against the in-house database with SHAFTS (**Figure 1a**)^{67, 68}. A set of 12 compounds were selected out by 3D similarity calculation for primary validation by fluorescence polarization (FP) assay with the FITC-labelled MLL-derived peptide MBM1. The results of FP assays indicated that loperamide, an antidiarrheal drug used for acute and chronic diarrhea as well as ileostomy, showed mild inhibition for menin-MBM1 complex ($IC_{50} = 69 \pm 3 \mu\text{M}$, **Figure 1b**). NMR Carr-Purcell-Meiboom-Gill (CPMG) and saturation transfer difference (STD) experiments provided evident evidence of the direct binding between loperamide and menin (**Figure 1c-d**) which makes us to conclude that loperamide binds directly to menin and disrupts the interactions of menin-MBM1 complex.

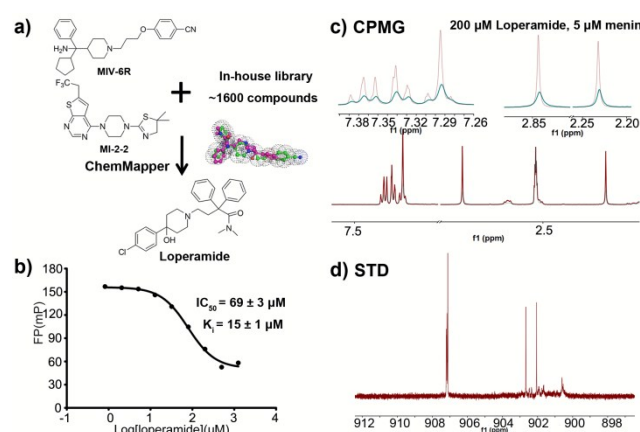


Figure 1. Seeking loperamide out for targeting menin-MLL interaction. **a)** The flowchart of scaffold hopping. **b)** FP result of loperamide. **c-d)** CPMG and STD NMR experiments demonstrate the binding of loperamide to menin.

To understand the molecular details of how loperamide interacts with menin-MLL interface, molecular docking simulations were performed using Glide 5.5^{69, 70}. The results revealed that loperamide roughly occupies the binding sites of MBM1 peptides (**Figure 2a-b**), indicating that several regions of loperamide can be modified to make this compound fit into the binding pocket in a better way (**Figure 2c**). Using loperamide as a hit compound, chemical optimizations were performed to improve potencies (see below).

Structural Optimizations of Loperamide Scaffold

A series of derivatives were obtained by both similarity search and chemical synthesis (**Table 1**) to get a deeper understanding of structure activity relationship (SAR). After the validation of FP assay, we found that the quarterization of piperidin (R1 region in **Figure 2c**) or the substitution of piperidinring to piperazine totally abolished potency of the compounds (**DC_YM1**, **DC_YM7**, **Table 1**). Introduction of a double bond into the piperidin group, which yield 4-(4-(4-chlorophenyl)-5,6-dihydropyridin-1(2H)-yl)-*N,N*-dimethyl-2,2-diphenylbutanamide (**DC_YM6**), led to a 4-fold increase in activity ($IC_{50} = 18 \pm 2 \mu\text{M}$, **Table 1 and Supplementary Figure 2**). On the basis of these data, we concluded that 1,2,3,6-tetrahydropyridine is the preferred group in the linker region. Next, the dimethylacetamide group (R2 region in **Figure 2c**) at the head region was replaced with different acylamino groups to explore its role in activities. The inhibitory activity of 4-(4-(4-chlorophenyl)-5,6-dihydropyridin-1(2H)-yl)-*N*-methyl-2,2-diphenylbutanamide (**DC_YM2**), with hydrogen atom replacing one methyl group, was slightly weaker versus loperamide ($IC_{50} = 79 \pm 4 \mu\text{M}$, **Table 1**). Removal of two methyl groups resulted in decrease in activity with $IC_{50} > 200 \mu\text{M}$ (**DC_YM3**, **Table 1**) implying that alkyl groups at R2 position is important for inhibitory activity. Introduction of the preferred group

1,2,3,6-tetrahydropyridine at R1 position as well as the bulkier ethyl group at R2 position, yielded about 4-fold increase in activity ($IC_{50} = 16 \pm 2 \mu\text{M}$, **DC_YM8**, **Table 1**). We found that substitution of the dimethylacetamide group with ethanamine, which includes an alkyl hydrophobic group, 4-(4-(4-chlorophenyl)-5,6-dihydropyridin-1(2H)-yl)-2,2-diphenylbutan-1-amine (**DC_YM9**), also shows inhibition of the menin-MLL interactions ($IC_{50} = 26 \pm 3 \mu\text{M}$, **Table 1**). However, the replacement of acylamino groups with hydrophilic group nitrile or hydroxyl totally abolished the activity of inhibitors (**DC_YM4**, **DC_YM5**, **Table 1**), validating the essential role of hydrophobic substituents at R2 position in compounds.

As shown in **Figure 2a-b**, there are very few interactions between menin and the tail group region of loperamide (R3 region in **Figure 2c**), which gives us space for optimization. Replacement of chlorine atom with methoxy group in the tail region resulted in a modest ~ 1.5 -fold increase in IC_{50} value ($IC_{50} = 13 \pm 2 \mu\text{M}$, **DC_YM10**, **Table 2**), implying that extension of tail group with hydrophobic substituents can improve inhibitory activity. Introduction of hydrophilic group nitrile slightly decreased the inhibitory activity, validating the importance of hydrophobic substituents ($IC_{50} = 22 \pm 4 \mu\text{M}$, **DC_YM11**, **Table 2**). However, introducing phenyl rings which adopt a larger size reduced the inhibitory activity completely

due to steric clash (**DC_YM18-DC_YM20**, **Table 2**). Since there is a hydrogen bond formed between the nitrile group of **MIV-6R** and the indole nitrogen of W341 on menin⁵³, we explored weather introduction of hydrogen-bond acceptors at R3 region can improve activities. Consequently, the inhibitory activity of N,N-dimethyl-4-(4-(4-(methylsulfon-amido)-phenyl)-5,6-dihydropyridin-1(2H)-yl)-2,2-diphenylbutanamide (**DC_YM13**), with methane sulfonamide replacing the chlorine atom, was increased by about 3-fold ($IC_{50} = 5.9 \pm 0.4 \mu\text{M}$, **DC_YM13**, **Table 2**). Halogen bonding, a specific intermolecular interaction between a halogen atom and an electron-rich partner (O, N, S, or π), is a distinct class of hydrogen-bond-like interactions⁴⁵. Therefore, introducing a fluorine atom also lead to an improvement in activity ($IC_{50} = 7.6 \pm 2.1 \mu\text{M}$, **DC_YM12**, **Table 2**). As for **DC_YM14-DC_YM16**, the inhibitory activities were degraded in different degrees, probably due to formation of intramolecular hydrogen-bonds in these compounds. The binding pocket in menin that interacts with the tail region of inhibitors is negatively charged (**Figure 2a**) and replacement of R3 region with the negative-charged carboxyl completely abolished the interaction between menin and the compound (**DC_YM17**, **Table 2**). These results demonstrated that the binding affinity could be improved through introduction of proper hydrophobic substituents and hydrogen-bond acceptors at the tail region of inhibitors.

The binding mode of loperamide revealed that menin-loperamide interactions are mostly mediated by the hydrophobic contacts between protein and the head group region of compound (R4 region in **Figure 2c**). However, two benzene rings cannot fit into the F9 and P10 hydrophobic pockets very well (**Figure 2a**). Thus, one of the phenyl rings at the head region of loperamide was substituted with different groups to explore ways of improving its potency. As a result, cycloalkanes or chain hydrocarbons substituents both led to significant improvement of the inhibitory activity. Cyclopentyl was found to be the optimal group at this position while introducing a 2-fluoro or 3-fluoro to another phenyl ring led to decrease in activities (**DC_YM21-DC_YM23**, **Table 3**). Among these compounds, 4-(4-(4-chlorophenyl)-5,6-dihydropyridin-1(2H)-yl)-2-cyclopentyl-2-phenylbutan-1-amine exhibited about 30-fold increase in activity versus **DC_YM9** ($IC_{50} = 0.83 \pm 0.13 \mu\text{M}$, **DC_YM21**, **Table 3**). Molecular docking simulations were performed to investigate the binding mode between **DC_YM21** and menin. As shown in **Figure 3a**, the phenyl and cyclopentyl rings in the head group of **DC_YM21** overlaps with side chains of F9 and P10 in MLL, thus closely mimicking the interactions between menin and MLL. As guided by modifications on the tail group region (**Table 2**), the chlorine atom was replaced with fluorine atom and methane sulfonamide group resulting in increased inhibitory activities against the menin-MLL interactions (**DC_YM25-DC_YM26**, **Table 3**). Molecular modeling implies that the improved affinity is probably contributed by hydrogen bonds and

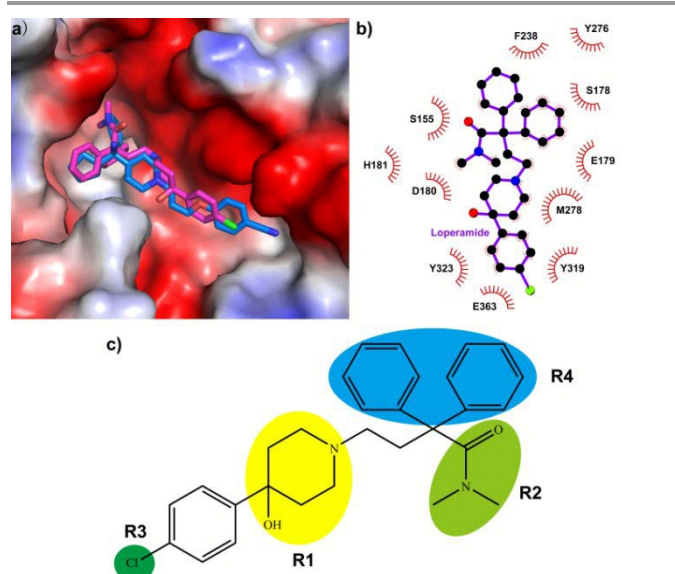
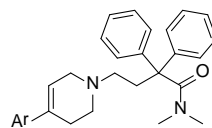


Figure 2. Binding mode of loperamide to menin cavity. a) Molecular modeling of loperamide/menin complex. The crystal structure of **MIV-6R** binding at active site in menin is also shown for comparison (PDB ID: 4GO8). Loperamide is colored in magenta, and **MIV-6R** is colored in blue. b) Schematic diagram showing interactions between loperamide and menin. Residues involved in the hydrophobic interactions are shown as starbursts. Molecular graphics figures were prepared with LigPlot⁺ program⁷¹. c) Four regions in loperamide to be modified by chemistry optimization.

Table 1. Structures and IC₅₀ values for loperamide and its derivatives

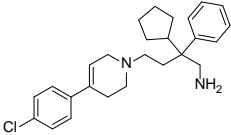
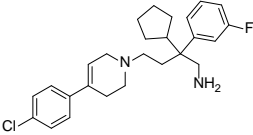
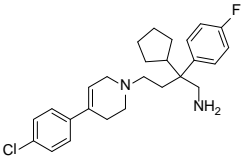
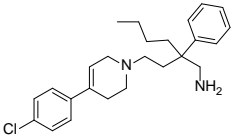
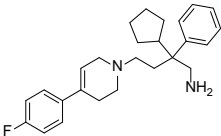
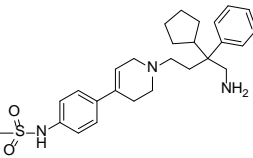
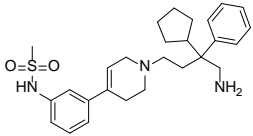
Compound	Structure	Ki (μM)	IC ₅₀ (μM)
Loperamide		15 ± 1	69 ± 3
DC_YM1		-	N.I.
DC_YM2		18 ± 1	79 ± 4
DC_YM3		-	> 200
DC_YM4		-	N.I.
DC_YM5		-	N.I.
DC_YM6		4.1 ± 0.5	18 ± 2
DC_YM7		-	N.I.
DC_YM8		3.5 ± 0.5	16 ± 2
DC_YM9		5.8 ± 0.8	27 ± 4

Table 2. Structures of loperamide-based analogues modified in the tail group region



Compound	Structure	K _i (μM)	IC ₅₀ (μM)
DC_YM10		2.7 ± 0.4	13 ± 2
DC_YM11		4.7 ± 0.9	22 ± 4
DC_YM12		1.6 ± 0.5	7.6 ± 2.1
DC_YM13		1.2 ± 0.1	5.9 ± 0.4
DC_YM14		39 ± 3	175 ± 13
DC_YM15		6.5 ± 0.7	30 ± 3
DC_YM16		21 ± 1	94 ± 5
DC_YM17		-	N.I.
DC_YM18		-	N.I.
DC_YM19		-	N.I.
DC_YM20		-	N.I.

Table 3. Structures and activities of analogues with substitution of alkyl group in the head region

Compound	Structure	K_i (μM)	IC_{50} (μM)
DC_YM21		0.08 ± 0.03	0.83 ± 0.13
DC_YM22		0.36 ± 0.05	2.1 ± 0.2
DC_YM23		0.59 ± 0.15	3.2 ± 0.7
DC_YM24		1.4 ± 0.3	6.9 ± 1.2
DC_YM25		0.05 ± 0.02	0.69 ± 0.07
DC_YM26		0.04 ± 0.01	0.66 ± 0.05
DC_YM27		0.88 ± 0.24	4.4 ± 1.1

N.I. refers to no inhibitory activity

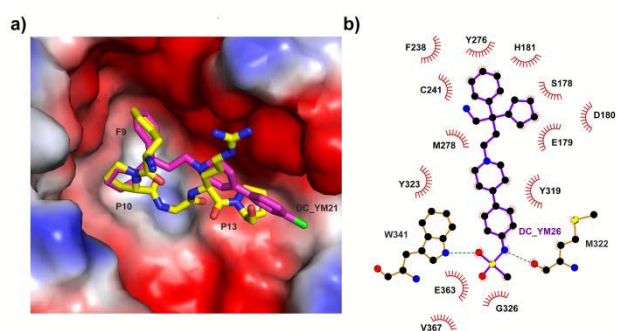


Figure 3. Binding mode of potent inhibitors. a) Molecular modeling of DC_YM21/menin complex. The crystal structure of MLL peptide binding at active site in menin is also shown for comparison (PDB code 4GQ6). DC_YM21 is colored in magenta, and MLL peptide is colored in yellow. b) Schematic diagram showing interactions between DC_YM26 and menin. Residues involved in the hydrophobic interactions are shown as starbursts, and hydrogen-bonding interactions are denoted by dotted green lines. Molecular graphics figures were prepared with LigPlot⁺ program⁷².

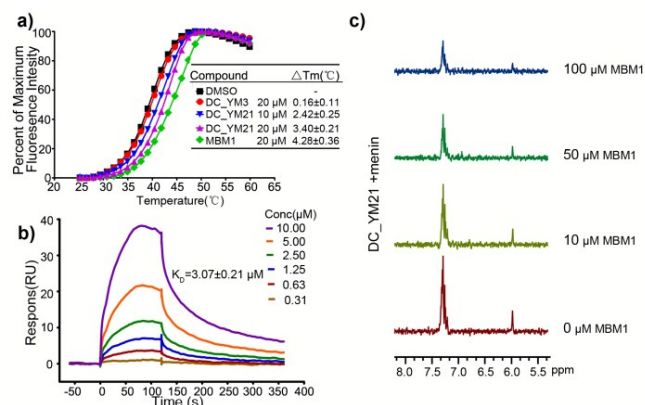


Figure 4. DC_YM21 binds to menin and disrupt menin-MLL interface in vitro. a) Changes in thermodynamic stability of menin upon binding of DC_YM21 and DC_YM3. b) Surface Plasmon Resonance (SPR) experiment of DC_YM21 binding to menin. c) Competition with MBM1 peptide in NMR STD experiments containing DC_YM21 (200 μ M) and menin (5 μ M).

hydrophobic interactions between the tail group of DC_YM26 and the binding pocket which is mainly formed by M322, E326, W341, and E363 (Figure 3b). Para-substitution of the R4 region is vital for inhibitory activity and meta-methane sulfonamide replacement decreased activity probably due to steric clashes, as compound DC_YM27 was much less active than DC_YM26. Overall, the structure-activity relationships (SAR) of menin-MLL inhibitors shed light on further chemical modification in order to improve inhibitory activity.

Inhibition of menin-MLL Interface in vitro

Taken both *in vitro* and *in vivo* behaviors into consideration, DC_YM21 was believed to be one of the most potent inhibitors against menin-MLL interface. DC_YM21 disrupted the menin-MBM1 complex with nanomolar activity ($IC_{50} = 0.83 \pm 0.13 \mu$ M) in the FP competition assay, which is only slight weaker than

DC_YM25 and DC_YM26 (Table 3). To determine the binding affinity of DC_YM21 with menin, the melting temperature (T_m value) of menin protein was first measured with a differential scanning fluorimetry assay. The presence of DC_YM21 at 10 μ M and 20 μ M both led to significant increases in T_m values ($\Delta T_m = 2.42 \pm 0.25^\circ$ C and $3.40 \pm 0.21^\circ$ C respectively, Figure 4a), indicating the direct interactions between the compound and menin in the dose-dependent manner. In contrast, the analogue of DC_YM21, DC_YM3, which displayed poor activity in FP assay (Table 1), caused no shift in the differential scanning fluorimetry assay (Figure 4a). The equilibrium dissociation constant value of DC_YM21 and menin was also determined to be $3.07 \pm 0.21 \mu$ M (Figure 4b) by a Surface Plasmon Resonance (SPR) experiment.

In order to confirm that DC_YM21 binds directly to menin and competes with MLL, competition saturation transfer difference (STD) NMR experiments were also performed using the MBM1 peptide. A significant and dose-dependent decrease in the STD effect of DC_YM21 was detected upon adding the MBM1 at the final concentration of 10 μ M, 50 μ M, and 100 μ M (Figure 4c), indicating that DC_YM21 binds menin at the same site of MBM1 binding.

Disrupting the Menin and MLL Fusion Protein Interaction in Cells by DC_YM21

To test the capacity of potent compounds in disrupting the menin and MLL fusion protein interaction in cells, co-immunoprecipitation experiments were performed in HEK293 cells transfected with flag-MLL_N. Menin was expressed endogenously in a high level and could be co-immunoprecipitated with Flag-MLL_N in the DMSO treated sample (Figure 5a). After treatment with DC_YM21 in the indicated concentration for 12 h, less menin protein was detected in co-immunoprecipitation samples (Figure 5a), demonstrating the effective disrupting of menin-MLL fusion protein interactions in human cells.

Growth Inhibition and Cell Cycle Arrest in Leukemia Cells

Inhibitors targeting the menin-MLL fusion protein interaction are supposed to cause cell growth inhibition and induce cell cycle arrest in cells with MLL fusions^{43,44,47}. Several leukemia cells were chosen and treated with potent inhibitors to assess the effect of growth inhibition.

Treatment with DC_YM21 after 7 days effectively blocked the proliferation of MV4;11 and KOPN-8 cells, with half-maximal growth inhibitory concentration (GI_{50}) values of $1.67 \pm 0.51 \mu$ M and $2.08 \pm 0.42 \mu$ M respectively, whereas minimal effect on proliferation was observed in leukemia cells without MLL translocation (Figure 5b). In contrast, DC_YM3 showed a much weaker effect on proliferation of MV4;11 cells (Figure 5c). Besides, impacts of several other potent molecules as well as the reported inhibitor MI-2-2 were measured in the MV4;11

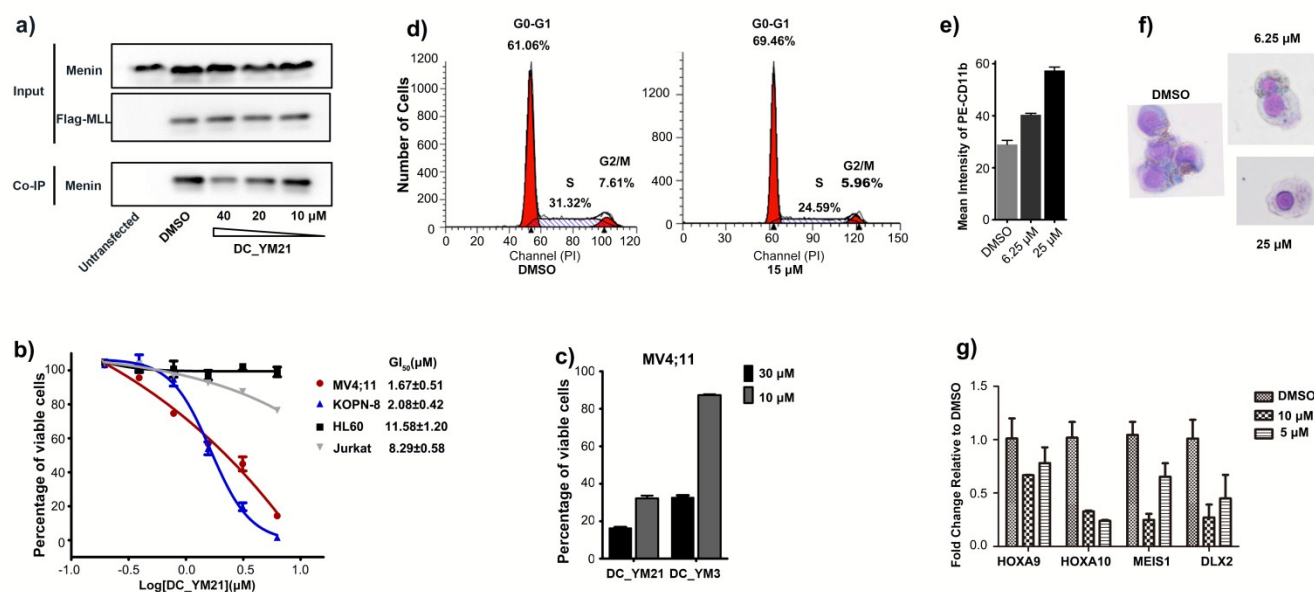


Figure 5. Menin-MLL inhibitor DC_YM21 displays significant biological activities. **a)** HEK293 cells were transfected with Flag-MLL₁₋₁₆₇ and co-immunoprecipitation experiment was performed after treatment with inhibitors for 12 h. **b)** AlamarBlue cell viability assay of human leukemia cells with or without MLL-fusion translocations after 7 days' treatment with DC_YM21. The experiment was performed three times. **c)** AlamarBlue cell viability assay of MV4;11 cells after 3 days' treatment with DC_YM21 and DC_YM3. The experiment was performed three times. **d)** Effect of DC_YM21 on cell cycle progression measured by FACS in MV4;11 cells after 2 days' treatment. **e)** Quantification of CD11b expression in MV4;11 cells treated for 7 days with DC_YM21. Data represent the mean values for quad-ruplicates \pm SD. **f)** Wright-Giemsa-stained cytopins for MV4;11 cells after 10 days' treatment. The experiment was performed four times. **g)** Expression of the *Hox* genes and *MEIS1*, *DLX2* genes by quantitative Real-Time PCR in MV4;11 cells treated for 3 days with DC_YM21 referenced to DMSO-treated samples. Data represent the mean values for duplicates \pm SD.

cells (Supplementary Table2), indicating the same level activity of these compounds in cellular responses causing. The effect of DC_YM21 on cell cycle progression was measured by FACS analysis in MV4;11 cells (Figure 5d). DC_YM21 caused an increase in the number of cells in the G0/G1 phase at the concentration of 15 μ M by 2 days, and a substantial decrease in the S phase was observed. Thus, these results validated the selective killing of MLL leukemia cells by the menin-MLL inhibitors DC_YM21.

Cell Differentiation and Downregulation of MLL Fusion Target Genes Induced by DC_YM21

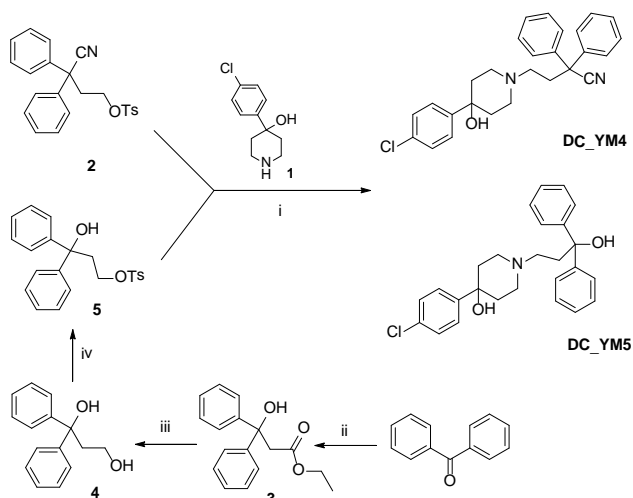
Having measured the selective growth inhibition effect of compounds, we further assessed the impact on induction of differentiation in two MLL leukemia cells MV4;11 and KOPN-8 (Figure 5e-f and Supplementary Figure 3A). After treatment with DC_YM21, a marked morphology change from primitive blasts to more mature myeloid cells was observed (Figure 5f). A significant increase in cells positive for CD11b, a myeloid differentiation marker, was detected after 7 days' treatment of MV4;11 cells (Figure 5e). Together, these results reveal that disrupting the interaction of menin-MLL fusion protein by DC_YM21 relieves the differentiation block induced by MLL fusion proteins in human MLL leukemia cells.

Upregulating of HOX cluster genes and HOX cofactor MEIS1 is symbolic in human MLL leukemia cells^{30,31}. MV4;11 cells were treated with DC_YM21 at various concentrations and the Real-Time PCR experiment was performed to monitor several MLL-fusion protein target genes. Particularly, homeobox genes *HOXA10* and *MEIS1*, as well as one of the downstream targets *DLX2*⁴⁸ were profoundly decreased upon treatment with DC_YM21 compared with the DMSO control sample (Figure 5g). *HOXA9* also showed a mild down-regulation effect.

Chemistry

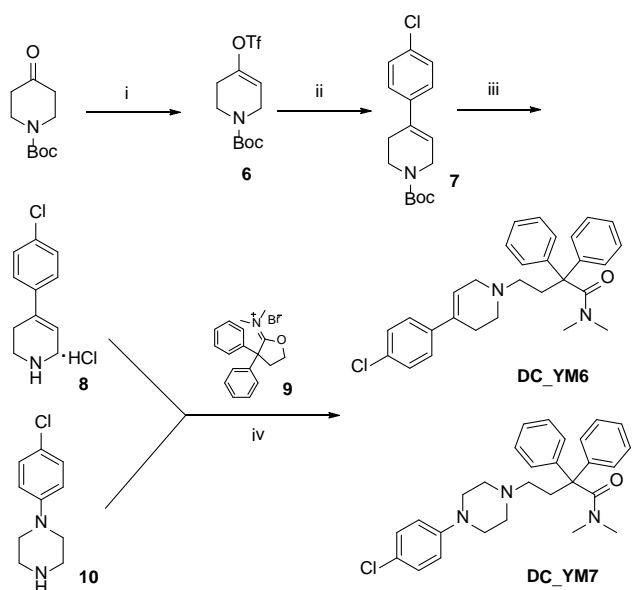
A total of 24 loperamide-based analogues were synthesized for optimization of inhibitory activity against the menin-MLL interaction. Firstly, to identify the role of amide in loperamide, analogues having a cyano or hydroxyl in place of the amide group were readily synthesized. As outline in Scheme 1, the first route employs substitution with commercially available 4-(4-chlorophenyl)-4-hydroxypiperidine (**1**) and 4-bromo-2,2-diphenylbutanenitrile (**2**) yielding DC_YM4 in high yield. Similarly, tosylate (**5**) was synthesized in three steps starting from the benzophenone⁷³, followed by subsequent substitution with **1** to afford the desired analogue DC_YM5.

Full experimental details can be found within **Supporting Information**.



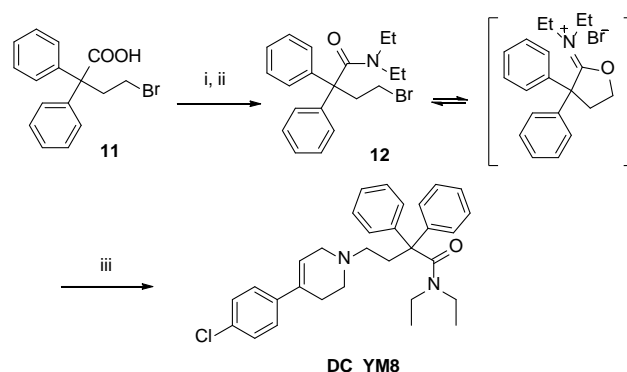
Scheme 1 Synthesis of Compound **DC_YM4** and **DC_YM5**. Reagents and conditions: (i) 1, Na₂CO₃, MeCN, 80 °C, 4 h, 80-83%; (ii) LDA, EA, -78 °C, 2 h, 95%; (iii) LiAlH₄, THF, 0 °C, 1 h, 90%; (iv) TsCl, pyridine, 0 °C, 4 h, 72%.

Next, we intend to remove the hydroxyl of piperidin ring and introduce double bond or nitrogen atom to build the tetrahydropyridine or piperazine scaffold and a strategy with Suzuki coupling as a key step⁷⁴ was employed. Starting from the commercially available Boc-protected piperidone followed by trifluoromethylsulfonylation, we were able to obtain 4-chlorophenyl-1,2,3,6-tetrahydropyridine core and subsequent deprotection provided **8** as hydrochloride salt. Substitution with an important intermediate **9** (commercially available or prepared according to the previous work⁷⁵) using Na₂CO₃ as a weak base to form **DC_YM6** and **DC_YM7**, respectively, Scheme 2.



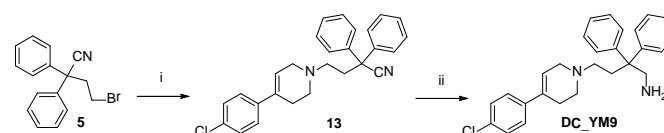
Scheme 2 Synthesis of Compound **DC_YM6** and **DC_YM7**. Reagents and conditions: (i) LDA, 1,1,1-trifluoro-N-phenyl-N-(trifluoromethyl sulfonyl)methane sulfonamide, -78 °C, 3 h, 92%; (ii) 4-chlorobenzeneboronic acid, PdCl₂(PPh₃)₂, NaHCO₃, THF, reflux, 2 h, 95%; (iii) hydrogen chloride (gas), EA, r.t., 1 h, 90%; (iv) 9, Na₂CO₃, MeCN, 80 °C, 4 h, 80-82%.

Synthesis of **DC_YM8** was performed according to Scheme 3. Acyl chlorination of 4-bromo-2,2-diphenylbutyric acid (**11**) proceeded efficiently with SOCl₂ producing the diphenylbutanoyl chloride, which was then subjected to diethylamine to afford *N,N*-diethyl-substituted amide (**12**)⁷⁵. Similar approach was employed for synthesis of **DC_YM8**, which substitution with 4-(4-chlorophenyl)-1,2,3,6-tetrahydropyridine hydrochloride salt (**8**). The process was optimized to provide good overall yield of 68% over three steps.

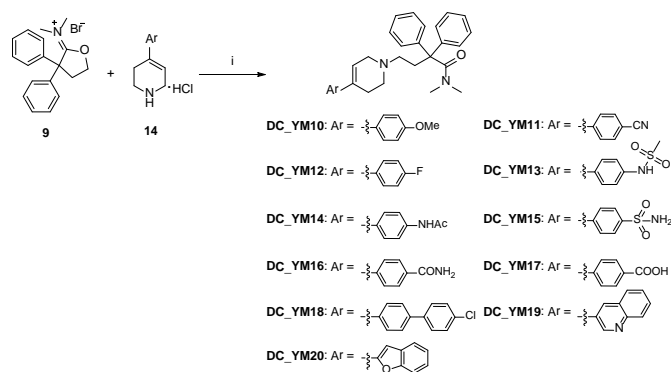


Scheme 3 Synthesis of Compound **DC_YM8**. Reagents and conditions: (i) 11, SOCl₂, CHCl₃, reflux, 4 h; (ii) diethylamine, Na₂CO₃, PhMe/H₂O, 0~5 °C, 2 h; (iii) 8, Na₂CO₃, MeCN, 80 °C, 4 h, 3 steps 68%.

For preparation of **DC_YM9**, we explored the possibility of removing carbonyl group on head region. Thus, reduction of nitrile to primary amine gave us a feasible method. However, initial screening of various reduction conditions, including borohydride, LiAlH₄ or borane complexes, we failed to get the desired product due to the inert nitrile in compound **13**. Finally, lewis acid-assisted reduction strategy was accomplished utilizing fresh preparation LiAlH₄-AlCl₃ complex, which was described by K. May *et al.*⁷⁶, that with AlCl₃ adding into a solution of LiAlH₄ in THF and the reductive reaction should perform at reflux temperature, successfully producing analogue **DC_YM9** in mild yield (Scheme 4).

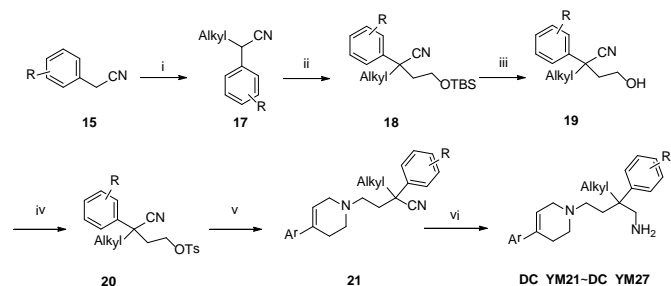


Scheme 4 Synthesis of Compound **DC_YM9**. Reagents and conditions: (i) 8, Na₂CO₃, MeCN, 80 °C, 4 h, 80%; (ii) LiAlH₄-AlCl₃, THF, r.t. to reflux, 7 h, 60%.



Scheme 5 Synthesis of Compound **DC_YM10**~**DC_YM20**. Reagents and conditions: (i) **9**, Na_2CO_3 , MeCN, 80°C , 4~6 h, 62-81%.

The synthesis of compounds **DC_YM10**~**DC_YM20**, with multiple aryl-substituents on tetrahydropyridine ring is depicted in Scheme 5. The 4-aryl substituted-1,2,3,6-tetrahydropyridine intermediates (**14**) involving polar or less-polar groups, polycyclic or heterocycle aromatic moieties were synthesized via the previously described Suzuki coupling, followed by substitution with the commercially available furaniminium bromide (**9**) to obtain the corresponding loperamide-based analogues with tail group region modified.



Scheme 6 Synthesis of Compounds **DC_YM21**~**DC_YM27**. Reagents and conditions: (i) Alkyl-Br **16**, NaNH_2 , Et_2O , reflux, 3 h, 83-90%; (ii) 2-(tert-butyldimethylsilyloxy)ethyl bromide, NaNH_2 , PhMe, 120°C , 3 h, 74-85%; (iii) TBAF, THF, r.t., 2 h, 85-90%; (iv) TsCl, pyridine, 0°C , 4 h, 85-88%; (v) aryl-substituted tetrahydropyridine **8** or **14**, pyridine, 0°C , 4 h, 64-72%; (vi) $\text{LiAlH}_4\text{-AlCl}_3$, THF, r.t. to reflux, 7~15 h, 41-57%

In an attempt to further modify on head region, synthesis of cyclopentyl aminomethyl tetrahydropyridine **DC_YM21**~**DC_YM27** is outlined in Scheme 6. Aryl acetonitriles **15** were initial deprotonated and reacted with alkyl bromide to give intermediate **17**, which followed by a second deprotonation and subjected to silyl ether-protected alkyl bromide, resulting compound **18**. Subsequent deprotection and tosylation to afford tosylate intermediates **20** in good yield, which were further reacted with aryl-substituted tetrahydropyridine (**14**) via the same substitution condition. The nitriles **21** were also reduced using $\text{LiAlH}_4\text{-AlCl}_3$ agent described for previous series to offer the analogues **DC_YM21**~**DC_YM27** with aminomethyl moiety.

Conclusions

View Article Online
DOI: 10.1039/C6OB01248E

MLL1 protein is the core component of MLL1 complex, possessing H3K4 methyltransferase activity. Translocation of MLL1 genes in leukemia translates with MLL fusion proteins, which are responsible for the upregulating expression of HOX genes and MEIS1, resulting in enhanced proliferation and blockage of hematopoietic differentiation^{30, 31}. Menin interacts with both wildtype MLL1 and MLL1 in MLL1-fusions and is reported to act as a co-factor in leukemic transformation^{42, 47}. Disrupting the interaction between menin and MLL1 by genetic or biochemical methods could abolish the oncogenic activity of MLL-fusion proteins^{42, 47}. Utilizing a shape-based scaffold hopping approach to analyze the recent small-molecule inhibitors of menin-MLL, we identified the antiarrheals loperamide to possess, previously unreported, mild inhibition of the menin-MLL interaction ($\text{IC}_{50} = 69 \pm 3 \mu\text{M}$). According to the binding mode analysis of loperamide at the menin-MLL interface, Structure-activity relationship studies were applied to obtain better inhibitors from this scaffold. In this work, we explored several changes in the piperidin group in the linker region, substitutions in the dimethylacetamide group at the head region, modifications in the tail group region as well as replacements of phenyl rings at the head region of loperamide scaffold. Several loperamide-derived analogues with nanomolar inhibitory activity for the menin-MLL interaction were obtained, showing the same level activities with the reported inhibitor **MI-2-2** in our fluorescence polarization assays and cell viability assays. Biochemical experiments demonstrated that **DC_YM21**, one of the potent novel scaffold molecules we developed from the antiarrheals loperamide, can specifically disrupt the menin-MLL interaction *in vitro* and *in vivo* by fitting into the menin cavity and competing with MLL. Treatment with **DC_YM21** results in cellular responses such as inhibition of proliferation, cell cycle arrest, induction of differentiation and down-regulation of MLL fusion target genes expression in human MLL leukemia cells, emphasizing on-target effects of menin-MLL inhibitor. Thus, we have provided molecules of a novel scaffold targeting menin-MLL interaction, and they may serve as new potential therapeutic agents for MLL leukemia. We also provided some clues for further menin-MLL inhibitors design and development in this work through repurposing the loperamide scaffold. However, the specific feature of menin in the complex interaction network^{41, 77} and the important physiological functions of MLL2 remain to be further studied. Inhibitors for menin-MLL interactions are supposed to serve as potential leads and powerful chemical biology probes for many other diseases beyond leukemia.

Experimental

Chemistry: General Information. Commercially available chemicals were used without further purification. All products were characterized by their NMR and MS spectra. Mass spectra and high-

resolution mass spectra were measured on a Finnigan MAT-95 mass spectrometer. Melting points (uncorrected) were determined using a SGWX-4B micro melting point apparatus. ^1H and ^{13}C NMR spectra were determined on Bruker AM-300, Bruker AM-400, Bruker AM-500 instruments using tetramethylsilane as internal reference. Data are presented as follows: chemical shift, multiplicity (s = singlet, br s = broad singlet, d = doublet, br d = broad doublet, t = triplet, m = multiplet), J = coupling constant in hertz (Hz). Silica gel 60H (200-300 mesh) manufactured by Qingdao Haiyang Chemical Group Co. (China) was used for general chromatography.

Procedures for Synthesis of Compounds. Synthesis of presented compounds was performed according to Schemes 1-6. Full experimental procedures, analytical data, and NMR spectra of compounds reported here can be found within Supporting Information. Synthesis and analytical data for representative compounds from *N,N*-dimethyl-2,2-diphenylbutanamide (DC_YM6 and DC_YM10 to DC_YM20) and 2-alkyl-2-arylbutan-1-amine (DC_YM21 to DC_YM27) classes are provided below.

Typical Experimental Procedure A (step 1 to step 4) for Synthesis of DC_YM6 and DC_YM10 to DC_YM20 using various of 4-aryl substituted-1,2,3,6-tetrahydropyridine (taking DC_YM6 as an example):

Step 1: To a solution of diisopropylamine (0.7 mL) in THF (10 mL) was added *n*-butyllithium solution in hexane (3.1 mL, 1.6 M in hexane) at -78°C . The mixture was stirred at -78°C for 15 min to get a LDA solution, and then 1-Boc-4-piperidone (1.0 g, 5.02 mmol) in THF (10 mL) was slowly added to the reaction mixture at -78°C . After 20 min, a solution of 1,1,1-trifluoro-*N*-phenyl-*N*-(trifluoromethylsulfonyl) methane sulfonamide (1.8 g, 5.02 mmol) in THF (10 mL) was slowly added to the mixture. The reaction mixture was stirred at 0°C for 3 h. The reaction was quenched with saturated NH_4Cl solution and extracted with EtOAc. The combined organic layers were washed with brine, and dried over Na_2SO_4 , and concentrated. The residue was purified by column chromatography with petroleum ether/ethyl acetate (10/1, v/v) to obtain the compound **6** (92% yield); LRMS (EI) m/z 331 $[\text{M}]^+$; ^1H NMR (300 MHz, CDCl_3) δ 5.80-5.72 (m, 1H), 4.06-4.02 (m, 2H), 3.63 (t, J = 5.6 Hz, 2H), 2.48-2.40 (m, 2H), 1.47 (s, 9H).

Step 2: To a solution of enol triflate **6** (331 mg, 1 mmol) in THF (4 mL) were added 4-chlorobenzenboronic acid (187 mg, 1.2 mmol), saturated NaHCO_3 solution (1 mL) and $\text{PdCl}_2(\text{PPh}_3)_2$ (14 mg, 0.02 mmol), and the mixture was stirred at reflux for 2 h. The mixture was diluted with EtOAc and the aqueous layer was separated and extracted with EtOAc. The organic layers were combined, washed with brine, dried over Na_2SO_4 and concentrated under reduced pressure. The residue was purified by flash column chromatography (petroleum ether/ethyl acetate = 2/1) to give compound **7** (95%); LRMS (EI) m/z 293 $[\text{M}]^+$; ^1H NMR (400 MHz, CDCl_3) δ 7.34-7.27 (m, 4H), 6.01 (brs, 1H), 4.06 (brs, 2H), 3.63 (brs, 2H), 2.47 (brs, 2H), 1.48 (s, 9H).

Step 3: A round-bottom flask was placed a solution of compound **7** (293 mg, 1 mmol) in ethyl acetate (5 mL), hydrogen chloride (gas) was bubbled through the solution and the resulting mixture was stirred for 1 h at room temperature. The formed precipitate was collected by filtration and dried to yield 206 mg (90%) of a white solid **8**; LRMS (EI) m/z 229 $[\text{M}]^+$.

Step 4: A solution of compound **8** (55 mg, 0.24 mmol) in CH_3CN (5 mL) was added dihydro-*N,N*-dimethyl-3,3-diphenyl-2(3H)-furaniminium bromide (**9**, 65 mg, 0.19 mmol) and Na_2CO_3 (60 mg, 0.57 mmol), and the mixture was stirred at 80°C for 4h. Then the solvent was removed in vacuo. The residue was diluted with EtOAc and washed with water. The organic layers were combined, washed with brine, dried over Na_2SO_4 and concentrated under reduced pressure. The residue was purified by flash column chromatography (dichloromethane/methanol = 20/1) to give compound **DC_YM6** (80%);

4-(4-(4-chlorophenyl)-3,6-dihydropyridin-1(2H)-yl)-*N,N*-dimethyl-2,2-diphenylbutanamide (DC_YM6)

Yield, 80%; mp $130 - 132^\circ\text{C}$; ^1H NMR (300 MHz, CDCl_3) δ 7.45-7.33 (m, 8H), 7.31-7.22 (m, 6H), 5.96-5.91 (m, 1H), 3.18-3.11 (m, 2H), 2.98 (brs, 3H), 2.69 (t, J = 5.6 Hz, 2H), 2.60-2.46 (m, 4H), 2.33 (brs, 3H), 2.32-2.21 (m, 2H); ^{13}C NMR (100 MHz, CDCl_3) δ 173.4, 140.7, 139.3, 133.7, 132.4, 128.3, 128.2, 128.0, 126.7, 126.1, 122.7, 59.7, 55.4, 53.1, 50.2, 42.6, 39.1, 37.2, 28.0; HRMS (EI) calcd. for $\text{C}_{29}\text{H}_{31}\text{ClN}_2\text{O}$ $[\text{M}]^+$: 458.2125. Found: 458.2122.

DC_YM10 to DC_YM20 were prepared according to the procedure A, step 4. To a stirred equimolecular suspension of dihydro-*N,N*-dimethyl-3,3-diphenyl-2(3H)-furaniminium bromide (**9**, 0.2 mmol), 4-substituted aryl-1,2,3,6-tetrahydropyridine intermediates (**14**, 0.25 mmol) and Na_2CO_3 , then the mixture was stirred at 80°C for 4-6 h. After general work up, the residue was purified by flash column chromatography to give compound. 4-(4-methoxyphenyl)-1,2,3,6-tetrahydropyridine **14a** for **DC_YM10**, 4-(1,2,3,6-tetrahydropyridin-4-yl)benzotrile **14b** for **DC_YM11**, 4-(4-fluorophenyl)-1,2,3,6-tetrahydropyridine **14c** for **DC_YM12**, *N*-(4-(1,2,3,6-tetrahydropyridin-4-yl)phenyl)methanesulfonamide **14d** for **DC_YM13**, *N*-(4-(1,2,3,6-tetrahydropyridin-4-yl)phenyl)acetamide **14e** for **DC_YM14**, 4-(1,2,3,6-tetrahydropyridin-4-yl)benzenesulfonamide **14f** for **DC_YM15**, 4-(1,2,3,6-tetrahydropyridin-4-yl)benzoic acid **14g** for **DC_YM16**, 4-(1,2,3,6-tetrahydropyridin-4-yl)benzamide **14h** for **DC_YM17**, 4-(4'-chloro-[1,1'-biphenyl]-4-yl)-1,2,3,6-tetrahydropyridine **14i** for **DC_YM18**, 3-(4-(1,2,3,6-tetrahydropyridin-4-yl)phenyl)quinolone **14j** for **DC_YM19**, 4-(4-(benzofuran-2-yl)phenyl)-1,2,3,6-tetrahydropyridine **14k** for **DC_YM20**. The purity of the synthesized compounds was determined to be greater than 95% by HPLC analysis [HPLC: column, YMC-Triart C18, 250 mm \times 4.6 mm, 5 μm ; solvent system, MeOH – 0.5 % $\text{NH}_3\cdot\text{H}_2\text{O}$ and water – 0.5 % $\text{NH}_3\cdot\text{H}_2\text{O}$ with gradient elution; flow rate, 1.0 mL/min; UV detection, 210

or 254 nm; oven, 20 °C. Agilent 1100, Agilent Technologies, California, USA]. Detailed HPLC analysis data of the synthesized compounds are displayed in Table S3 Supporting Information.

4-(4-(4-methoxyphenyl)-5,6-dihydropyridin-1(2H)-yl)-*N,N*-dimethyl-2,2-diphenylbutanamide (DC_YM10)

Yield, 76%; mp 170 – 172 °C; ¹H NMR (300 MHz, CDCl₃) δ 7.43-7.33 (m, 8H), 7.31-7.23 (m, 4H), 6.85-6.77 (m, 2H), 5.81 (s, 1H), 3.76 (s, 3H), 3.42 (m, 2H), 2.94 (m, 5H), 2.73-2.60 (m, 4H), 2.52 (m, 2H), 2.29 (s, 3H); ¹³C NMR (150 MHz, CDCl₃) δ 173.4, 159.7, 144.6, 135.1, 130.8, 129.7, 129.3, 129.1, 128.0, 127.9, 127.7, 126.3, 113.9, 112.6, 59.8, 55.3, 53.83, 50.2, 48.8, 39.2, 39.1, 37.2, 23.5; HRMS (EI) calcd. for C₃₀H₃₄N₂O₂ [M]⁺: 454.2620. Found: 454.2615.

4-(4-(4-cyanophenyl)-5,6-dihydropyridin-1(2H)-yl)-*N,N*-dimethyl-2,2-diphenylbutanamide (DC_YM11)

Yield, 70%; mp 175 – 177 °C; ¹H NMR (300 MHz, CDCl₃) δ 7.55 (d, *J* = 8.5 Hz, 2H), 7.46-7.33 (m, 10H), 7.31-7.25 (m, 2H), 6.12 (s, 1H), 3.13-3.07 (m, 2H), 2.99 (s, 3H), 2.62 (t, *J* = 5.7 Hz, 2H), 2.55-2.41 (m, 4H), 2.33 (s, 3H), 2.23-2.13 (m, 2H); ¹³C NMR (125 MHz, CDCl₃) δ 173.5, 145.3, 140.7, 133.6, 132.1, 128.4, 128.1, 126.8, 125.4, 119.1, 110.2, 59.8, 55.4, 53.2, 50.0, 42.8, 39.2, 37.2, 27.8; HRMS (EI) calcd. for C₃₀H₃₁N₃O [M]⁺: 449.2467. Found: 449.2462.

4-(4-(4-fluorophenyl)-5,6-dihydropyridin-1(2H)-yl)-*N,N*-dimethyl-2,2-diphenylbutanamide (DC_YM12)

Yield, 81%; mp 134 – 136 °C; ¹H NMR (300 MHz, CDCl₃) δ 7.38 (m, 8H), 7.35-7.25 (m, 3H), 7.12-6.80 (m, 3H), 5.85 (s, 1H), 3.29 (s, 2H), 2.98 (brs, 3H), 2.85 (t, *J* = 5.6 Hz, 2H), 2.58 (m, 4H), 2.45-2.35 (m, 2H), 2.31 (brs, 3H); ¹³C NMR (125 MHz, CDCl₃) δ 173.4, 162.0 (d, *J* = 244.1 Hz), 140.49, 136.7 (d, *J* = 3.0 Hz), 134.1, 128.6, 128.5, 128.1, 126.8, 126.5, 126.4, 125.3, 120.9, 115.1, 114.9, 59.7, 55.2, 52.8, 50.0, 42.1, 39.2, 37.1, 27.6; HRMS (EI) calcd. for C₂₉H₃₁FN₂O [M]⁺: 442.2420. Found: 442.2414.

***N,N*-dimethyl-4-(4-(4-(methylsulfonamido)phenyl)-5,6-dihydropyridin-1(2H)-yl)-2,2-diphenylbutanamide (DC_YM13)**

Yield, 62%; mp 154 – 156 °C; ¹H NMR (300 MHz, DMSO-*d*₆) δ 9.74 (brs, 1H), 7.45-7.21 (m, 12H), 7.12 (d, *J* = 8.7 Hz, 2H), 5.98 (s, 1H), 2.93 (s, 3H), 2.87 (m, 4H), 2.46-2.16 (m, 10H), 2.06-1.96 (m, 2H); ¹³C NMR (125 MHz, DMSO-*d*₆) δ 172.7, 141.6, 137.6, 136.2, 133.6, 128.8, 128.2, 127.0, 125.8, 121.9, 120.1, 59.4, 55.4, 55.3, 53.3, 50.4, 41.7, 27.9; HRMS (EI) calcd. for C₃₀H₃₅N₃O₃S [M]⁺: 517.2399. Found: 517.2396.

4-(4-(4-acetamidophenyl)-5,6-dihydropyridin-1(2H)-yl)-*N,N*-dimethyl-2,2-diphenylbutanamide (DC_YM14)

Yield, 68%; mp 160 – 162 °C; ¹H NMR (300 MHz, DMSO-*d*₆) δ 9.92 (s, 1H), 7.49 (d, *J* = 8.7 Hz, 2H), 7.40-7.25 (m, 12H), 5.96 (s, 1H), 2.93-2.73 (m, 5H), 2.45-2.21 (m, 9H), 2.05-1.95 (m, 5H); ¹³C NMR (125 MHz, DMSO-*d*₆) δ 172.7, 168.6, 141.7, 138.7, 135.2, 133.7, 128.8, 128.2, 127.0, 125.1, 121.3, 119.2, 59.4, 55.5, 55.4, 53.4, 50.5, 41.7, 27.9, 24.5; HRMS (EI) calcd. for C₃₁H₃₅N₃O₂ [M]⁺: 481.2729. Found: 481.2731.

***N,N*-dimethyl-2,2-diphenyl-4-(4-(4-sulfamoylphenyl)-5,6-dihydropyridin-1(2H)-yl)butanamide (DC_YM15)**

Yield, 63%; mp 245 – 248 °C; ¹H NMR (300 MHz, DMSO-*d*₆) δ 7.74 (d, *J* = 8.5 Hz, 2H), 7.55 (d, *J* = 8.5 Hz, 2H), 7.45-7.24 (m, 12H), 6.22 (s, 1H), 3.01-2.75 (m, 5H), 2.48-2.18 (m, 9H), 2.10-1.99 (m, 2H); ¹³C NMR (125 MHz, DMSO-*d*₆) δ 172.7, 143.8, 142.7, 141.6, 133.4, 128.9, 128.2, 127.0, 126.2, 125.3, 59.4, 55.4, 53.3, 50.3, 41.7, 27.8; HRMS (EI) calcd. for C₂₉H₃₃N₃O₃S [M]⁺: 503.2243. Found: 503.2237.

4-(1-(4-(dimethylamino)-4-oxo-3,3-diphenylbutyl)-1,2,3,6-tetrahydropyridin-4-yl)benzamide (DC_YM16)

Yield, 73%; mp 143 – 145 °C; ¹H NMR (300 MHz, DMSO-*d*₆) δ 7.81 (d, *J* = 8.3 Hz, 2H), 7.47 – 7.25 (m, 14H), 6.18 (s, 1H), 3.00-2.80 (m, 5H), 2.48-2.18 (m, 9H), 2.10-2.00 (m, 2H); ¹³C NMR (125 MHz, DMSO-*d*₆) δ 172.7, 168.0, 143.2, 141.6, 133.7, 132.9, 128.9, 128.2, 128.1, 127.0, 124.6, 124.3, 59.4, 55.4, 55.3, 53.4, 50.4, 41.7, 27.8; HRMS (EI) calcd. for C₃₀H₃₃N₃O₂ [M]⁺: 467.2573. Found: 467.2576.

4-(1-(4-(dimethylamino)-4-oxo-3,3-diphenylbutyl)-1,2,3,6-tetrahydropyridin-4-yl)benzoic acid (DC_YM17)

Yield, 71%; mp 238 – 240 °C; ¹H NMR (300 MHz, DMSO-*d*₆) δ 11.22 (s, 1H), 7.91 (d, *J* = 8.4 Hz, 2H), 7.54 (d, *J* = 8.4 Hz, 2H), 7.50 – 7.32 (m, 10H), 6.24 (s, 1H), 3.75-3.42 (m, 6H), 2.91 (brs, 3H), 2.79-2.67 (m, 4H), 2.22 (brs, 3H); ¹³C NMR (125 MHz, DMSO-*d*₆) δ 172.6, 167.4, 142.7, 140.1, 139.9, 133.6, 130.4, 130.0, 129.3, 128.3, 128.2, 127.7, 12 5.3, 119.1, 59.6, 53.6, 50.1, 48.0, 39.0, 38.4, 37.1, 23.8; HRMS (EI) calcd. for C₃₀H₃₂N₂O₃ [M]⁺: 468.2413. Found: 468.2414

4-(4-(4'-chloro-[1,1'-biphenyl]-4-yl)-5,6-dihydropyridin-1(2H)-yl)-*N,N*-dimethyl-2,2-diphenylbutanamide (DC_YM18)

Yield, 76%; mp 161 – 163 °C; ¹H NMR (500 MHz, CDCl₃) δ 7.54-7.36 (m, 16H), 7.30 (t, *J* = 7.2 Hz, 2H), 6.06 (s, 1H), 3.11 (d, *J* = 2.3 Hz, 2H), 3.01 (brs, 3H), 2.65 (t, *J* = 5.5 Hz, 2H), 2.59-2.47 (m, 4H), 2.36 (brs, 3H), 2.22 (m, 2H); ¹³C NMR (125 MHz, CDCl₃) δ 173.5, 140.9, 140.3, 139.3, 138.2, 134.3, 133.2, 128.9, 128.4, 128.2, 126.7, 126.7, 125.4, 122.6, 59.8, 55.5, 53.3, 50.4, 42.7, 38.9, 37.3, 28.2; HRMS (EI) calcd. for C₃₅H₃₅ClN₂O [M]⁺: 534.2438. Found: 534.2433.

***N,N*-dimethyl-2,2-diphenyl-4-(4-(quinolin-3-yl)-5,6-dihydropyridin-1(2H)-yl)butanamide (DC_YM19)**

Yield, 75%; mp 132 – 134 °C; ¹H NMR (300 MHz, DMSO-*d*₆) δ 9.03 (s, 1H), 8.18 (s, 1H), 7.93 (t, *J* = 8.2 Hz, 2H), 7.66 (t, *J* = 7.5 Hz, 1H), 7.54 (t, *J* = 7.4 Hz, 1H), 7.46-7.20 (m, 10H), 6.38 (s, 1H), 2.96 (m, 2H), 2.87 (brs, 3H), 2.49 (m, 4H), 2.40 (m, 2H), 2.27 (brs, 3H), 2.05 (m, 2H); ¹³C NMR (125 MHz, DMSO-*d*₆) δ 172.7, 148.6, 146.9, 141.6, 132.9, 131.8, 130.4, 129.4, 129.0, 128.9, 128.7, 128.3, 127.9, 127.2, 127.0, 125.0, 59.4, 55.4, 55.4, 53.4, 50.3, 41.7, 27.6; HRMS (EI) calcd. for C₃₂H₃₃N₃O [M]⁺: 475.2624. Found: 475.2622.

4-(4-(benzofuran-2-yl)-5,6-dihydropyridin-1(2H)-yl)-*N,N*-dimethyl-2,2-diphenylbutanamide (DC_YM20)

Yield, 65%; mp 140 – 142 °C; ¹H NMR (300 MHz, CDCl₃) δ 7.49-7.33 (m, 10H), 7.32 – 7.24 (m, 2H), 7.23 – 7.10 (m, 2H), 6.47 (s, 1H), 6.41 (s, 1H), 3.19-3.11 (m, 2H), 2.99 (brs, 3H), 2.65 (t, *J* = 5.6 Hz, 2H), 2.58 – 2.42 (m, 4H), 2.34 (brs, 3H), 2.26-2.18 (m, 2H); ¹³C NMR (125 MHz, CDCl₃) δ 173.5, 156.4, 154.5, 140.7, 129.0, 128.5, 128.1, 126.8, 125.5, 124.0, 122.6, 120.7, 110.8,

100.8, 59.8, 55.4, 52.7, 49.6, 42.5, 39.2, 37.2, 25.8; HRMS (EI) calcd. for $C_{31}H_{32}N_2O_2 [M]^+$: 464.2464. Found: 464.2467.

General procedure B (step 1 to step 6) for the synthesis of DC_YM21 to DC_YM27 (taking DC_YM21 as an example):

Step 1: A solution of 2-phenylacetonitrile (**15a**, 3 g, 25 mmol) in Et₂O (50 mL) was added bromocyclopentane (**16a** 2.7 mL) and NaNH₂ (1 g, 25 mmol), the mixture was refluxed for 3 h then quenched with water and extracted with EtOAc. The combined organic layers were washed with brine, and dried over Na₂SO₄, and concentrated. The residue was purified by column chromatography with petroleum ether/ethyl acetate (30/1, v/v) to obtain the compound **17a** (90% yield); LRMS (EI) *m/z* 185 [M]⁺; ¹H NMR (300 MHz, CDCl₃) δ 7.41-7.27 (m, 5H), 3.71 (d, *J* = 7.7 Hz, 1H), 2.38-2.24 (m, 1H), 1.94-1.80 (m, 1H), 1.76-1.63 (m, 3H), 1.62-1.48 (m, 3H), 1.40-1.28 (m, 1H).

Step 2: To a solution of compound **17a** (253 mg, 1.4 mmol) in PhMe (10 mL) was added 2-(tert-butyltrimethylsilyloxy)ethyl bromide (327 g, 1.4 mmol) and NaNH₂ (164 mg, 4.2 mmol), the mixture was stirred at 120°C for 3 h then quenched with water and extracted with EtOAc. The combined organic layers were washed with brine, and dried over Na₂SO₄, and concentrated. The residue was purified by column chromatography with petroleum ether/ethyl acetate (30/1, v/v) to obtain the compound **18a** (85% yield); LRMS (EI) *m/z* 343 [M]⁺; ¹H NMR (300 MHz, CDCl₃) δ 7.44-7.24 (m, 5H), 3.66-3.56 (m, 1H), 3.35-3.26 (m, 1H), 2.41-2.28 (m, 2H), 2.21-2.10 (m, 1H), 2.07-1.93 (m, 1H), 1.82-1.70 (m, 1H), 1.69-1.56 (m, 3H), 1.51-1.37 (m, 1H), 1.31-1.21 (m, 2H), 0.82 (s, 9H), -0.07 (d, *J* = 4.2 Hz, 6H).

Step 3: To a stirred solution of compound **18a** (343 mg, 1 mmol) in THF (5 mL) was added tetrabutylammonium fluoride (1 mL, 1M in THF), the reaction was stirred at room temperature for 2 h. The mixture was diluted with EtOAc and washed with water. The organic layers were combined, washed with brine, dried over Na₂SO₄ and concentrated under reduced pressure. The residue was purified by flash column chromatography (petroleum ether /acetone = 2/1) to give compound **19a** (90%); LRMS (EI) *m/z* 229 [M]⁺.

Step 4: The *p*-toluenesulfonyl chloride (191 mg, 1mmol) was added to the solution of the compound **19a** (206 mg, 0.9mmol) in dry pyridine (5mL) at 0°C under atmosphere of argon, and the mixture was stirred at 0°C for 4 h. The mixture was diluted with EtOAc and washed with hydrochloric acid (2M), the combined organic layers were washed with brine, and dried over Na₂SO₄, and concentrated. The residue was purified by column chromatography with petroleum ether/ethyl acetate (6/1, v/v) to obtain the compound **20a** (85% yield); LRMS (EI) *m/z* 383 [M]⁺; ¹H NMR (300 MHz, CDCl₃) δ 7.65 (d, *J* = 8.3 Hz, 2H), 7.37-7.25 (m, 7H), 3.96 (td, *J* = 9.8, 6.0 Hz, 1H), 3.75 (td, *J* = 9.8, 5.5 Hz, 1H), 2.53-2.41 (m, 4H), 2.38-2.25 (m, 2H), 1.99-1.87 (m, 1H), 1.81-1.69 (m, 1H), 1.62-1.53 (m, 3H), 1.49-1.35 (m, 1H), 1.28-1.20 (m, 2H).

Step 5: A solution of compound **20a** (383 mg, 1mmol) in CH₃CN (5mL) was added compound **8** (229 mg, 1mmol) and Na₂CO₃

(318 mg, 3mmol), and the mixture was stirred at 80°C for 4h. Then the solvent was removed in vacuo. The residue was diluted with EtOAc and washed with water. The organic layers were combined, washed with brine, dried over Na₂SO₄ and concentrated under reduced pressure. The residue was purified by flash column chromatography (petroleum ether /acetone = 3/1) to give compound **21a** (70%); LRMS (EI) *m/z* 404 [M]⁺; ¹H NMR (300 MHz, CDCl₃) δ 7.49-7.14 (m, 13H), 5.98 (s, 1H), 3.09-3.01 (m, 2H), 2.67-2.55 (m, 2H), 2.50-2.43 (m, 2H), 2.40-2.31 (m, 2H), 2.24-2.10 (m, 2H), 2.07-1.93 (m, 2H), 1.64-1.55 (m, 3H), 1.46-1.38 (m, 1H), 1.31-1.20 (m, 3H).

Step 6: LAH (0.15 mL, 2.4 M in THF) was slurried in anhydrous THF (5 mL), and the solution was cooled in an ice bath to 0°C under nitrogen. AlCl₃ (49 mg, 0.37 mmol) was dissolved in anhydrous THF (5mL). The AlCl₃ solution was added to the LAH slurry via an addition funnel over 15 min. Compound **21a** (50 mg, 0.12 mmol) was dissolved in anhydrous THF (5mL). This solution was added to the LAH/AlCl₃ mixture slowly. The resulting mixture was stirred at ambient temperature for 1 h and then heated to reflux for 7 h. When cooled to 0°C the reaction was quenched with water and extracted with Et₂O. The combined organic layers were washed with brine, and dried over Na₂SO₄, and concentrated. The residue was purified by column chromatography with dichloromethane/methanol (15/1, v/v) to obtain the compound **DC_YM21** (53%).

4-(4-(4-chlorophenyl)-3,6-dihydropyridin-1(2H)-yl)-2-cyclopentyl-2-phenylbutan-1-amine (DC_YM21)

Mp 195 – 197 °C; ¹H NMR (300 MHz, CDCl₃) δ 7.49-7.20 (m, 9H), 5.99 (s, 1H), 3.06 (s, 2H), 2.72-2.50 (m, 3H), 2.49 (m, 2H), 2.44-2.29 (m, 2H), 2.13 (d, *J* = 9.5 Hz, 3H), 1.65 (d, *J* = 12.3 Hz, 5H), 1.44 (s, 1H), 1.34-1.20 (m, 3H); ¹³C NMR (125 MHz, CDCl₃) δ 142.2, 139.2, 134.1, 132.7, 128.4, 128.1, 127.9, 126.2, 125.9, 122.2, 62.9, 53.7, 53.5, 50.6, 47.7, 47.0, 46.6, 31.3, 28.0, 27.1, 27.0, 24.5, 24.4; HRMS (EI) calcd. for C₂₆H₃₃ClN₂ [M]⁺, 408.2332. Found, 408.2325.

DC_YM22 to DC_YM27 were prepared according to the procedure B (step 1 to step 6). 2-(3-fluorophenyl) acetonitrile **15b** for **DC_YM22**, 2-(4-fluorophenyl) acetonitrile **15c** for **DC_YM23**, 1-bromopentane **16b** for **DC_YM24**, 4-(4-fluorophenyl)-1,2,3,6-tetrahydropyridine **14c** for **DC_YM25**, *N*-(4-(1,2,3,6-tetrahydropyridin-4-yl)phenyl)methanesulfonamide **14d** for **DC_YM26**, *N*-(3-(1,2,3,6-tetrahydropyridin-4-yl)phenyl)methanesulfonamide **14l** for **DC_YM27**. The purity of the synthesized compounds was determined to be greater than 95% by HPLC analysis [HPLC: column, YMC-Triart C18, 250 mm × 4.6 mm, 5 μ m; MeOH – 0.5 % NH₃.H₂O and water – 0.5 % NH₃.H₂O with gradient elution; flow rate, 1.0 mL/min; UV detection, 210 or 254 nm; oven, 20 °C. Agilent 1100, Agilent Technologies, California, USA]. Detailed HPLC analysis data of the synthesized compounds are displayed in Table S3 Supporting Information.

4-(4-(4-chlorophenyl)-5,6-dihydropyridin-1(2H)-yl)-2-cyclopentyl-2-(3-fluorophenyl) butan-1-amine (DC_YM22)

Mp 190 – 192 °C; ¹H NMR (300 MHz, CDCl₃) δ 7.31-7.23 (m, 5H), 7.06 (m, 2H), 6.90 (m, 1H), 6.03 (s, 1H), 3.20-3.00 (m, 4H), 2.70 (m, 2H), 2.54 (m, 2H), 2.41 (m, 2H), 2.10 (m, 2H), 1.73-1.49 (m, 3H), 1.39 (m, 5H), 1.01 (m, 3H); ¹³C NMR (125 MHz, CDCl₃) δ 162.9 (d, *J* = 242.9 Hz), 145.7 (d, *J* = 6.25 Hz), 139.2, 134.2, 132.8, 129.2 (d, *J* = 8.12 Hz), 128.5, 126.3, 123.7 (d, *J* = 2.12 Hz), 122.3, 115.3 (d, *J* = 21.6 Hz), 112.8 (d, *J* = 20.7 Hz), 53.7, 53.6, 50.8, 47.5, 47.2, 46.6, 31.4, 28.1, 27.1, 27.1, 24.5, 24.5; HRMS (EI) calcd. for C₂₆H₃₂ClFN₂[M]⁺, 426.2238. Found, 426.2240.

4-(4-(4-chlorophenyl)-5,6-dihydropyridin-1(2H)-yl)-2-cyclopentyl-2-(4-fluorophenyl)butan-1-amine (DC_YM23)

Mp 195 – 197 °C; ¹H NMR (300 MHz, CDCl₃) δ 7.36 – 7.23 (m, 6H), 7.03 (t, *J* = 8.3 Hz, 2H), 6.01 (d, *J* = 6.9 Hz, 1H), 3.13 (m, 3H), 2.69 (m, 2H), 2.56 (m, 3H), 2.41 (m, 2H), 2.02 (m, 2H), 1.85 (m, 1H), 1.63 (m, 3H), 1.40 (m, 4H), 1.15 (m, 3H); ¹³C NMR (125 MHz, CDCl₃) δ 161.1 (d, *J* = 243.7 Hz), 139.2, 138.1 (d, *J* = 2.5 Hz), 134.1, 132.7, 129.5 (d, *J* = 8.12 Hz), 128.4, 126.2, 122.2, 114.5 (d, *J* = 20.6 Hz), 53.7, 53.6, 50.8, 47.2, 46.7, 46.6, 31.4, 28.1, 27.0, 26.9, 24.4, 24.3; HRMS (EI) calcd. for C₂₆H₃₂ClFN₂[M]⁺, 426.2238. Found, 426.2242.

2-(2-(4-(4-chlorophenyl)-5,6-dihydropyridin-1(2H)-yl)ethyl)-2-phenylhexan-1-amine (DC_YM24)

Mp 170 – 173 °C; ¹H NMR (400 MHz, CDCl₃) δ 7.36-7.31 (m, 4H), 7.28 (m, 3H), 7.21 (m, 2H), 6.03 (m, 1H), 3.17-3.04 (m, 2H), 2.91 (s, 2H), 2.66 (t, *J* = 5.7 Hz, 2H), 2.52 (m, 2H), 2.36-2.20 (m, 2H), 1.98 (m, 2H), 1.72-1.64 (m, 2H), 1.29 (m, 4H), 1.17-1.07 (m, 2H), 0.88 (t, *J* = 7.3 Hz, 3H); ¹³C NMR (150 MHz, CDCl₃) δ 145.5, 139.4, 134.2, 132.8, 128.5, 126.8, 126.3, 126.0, 122.5, 53.6, 53.5, 50.7, 49.2, 44.8, 34.9, 32.2, 28.2, 25.8, 23.6, 14.2; HRMS (EI) calcd. for C₂₅H₃₃ClN₂[M]⁺, 396.2332. Found, 396.2321.

2-cyclopentyl-4-(4-(4-fluorophenyl)-5,6-dihydropyridin-1(2H)-yl)-2-phenylbutan-1-amine (DC_YM25)

Mp 210 – 212 °C; ¹H NMR (400 MHz, CDCl₃) δ 7.36 (m, 4H), 7.24 (m, 3H), 6.95 (t, *J* = 8.6 Hz, 2H), 6.51 (brs, 2H), 5.84 (s, 1H), 3.33 (d, *J* = 13.6 Hz, 1H), 3.17 (dd, *J* = 32.6, 15.1 Hz, 2H), 3.03 (d, *J* = 16.0 Hz, 1H), 2.88 (m, 1H), 2.68 (m, 1H), 2.60-2.44 (m, 4H), 2.34 (d, *J* = 15.7 Hz, 1H), 2.12-2.00 (m, 2H), 1.36 (m, 6H), 1.04 (m, 2H); ¹³C NMR (125 MHz, CDCl₃) δ 162.2 (d, *J* = 245 Hz), 139.9, 136.8 (d, *J* = 3.75 Hz), 134.7, 128.6, 127.8, 126.9 (d, *J* = 6.25 Hz), 126.7, 120.3, 115.3, 115.1, 52.9, 52.6, 50.4, 49.8, 47.2, 44.7, 32.4, 27.4, 27.2, 27.0, 24.6, 24.5; HRMS (EI) calcd. for C₂₆H₃₃FN₂[M]⁺, 392.2628. Found, 392.2623.

N-(3-(1-(4-amino-3-cyclopentyl-3-phenylbutyl)-1,2,3,6-tetrahydropyridin-4-yl)phenyl)methanesulfonamide (DC_YM26)

Mp 215 – 217 °C; ¹H NMR (500 MHz, CDCl₃) δ 7.32 (m, 4H), 7.18 (m, 5H), 5.97 (s, 1H), 3.31 (d, *J* = 13.4 Hz, 1H), 3.17 (dt, *J* = 27.1, 13.8 Hz, 3H), 2.93 (s, 3H), 2.76 (s, 1H), 2.65 (s, 1H), 2.49 (m, 4H), 2.33 – 1.94 (m, 4H), 1.39 (m, 5H), 1.08 (m, 3H); ¹³C NMR (125 MHz, CDCl₃) δ 141.5, 136.7, 136.6, 133.9, 128.0, 127.9, 125.9, 125.7, 120.7, 120.6, 53.5, 53.3, 50.4, 48.3, 47.1, 46.0, 39.0, 31.0, 27.7, 26.9, 26.7, 24.3, 24.2; HRMS (EI) calcd. for C₂₇H₃₇N₃O₂S[M]⁺, 467.2606. Found, 467.2603.

N-(3-(1-(4-amino-3-cyclopentyl-3-phenylbutyl)-1,2,3,6-tetrahydropyridin-4-yl)phenyl)methanesulfonamide (DC_YM27)

Mp 210 – 213 °C; ¹H NMR (400 MHz, CDCl₃) δ 7.40 (t, *J* = 7.7 Hz, 2H), 7.28 (d, *J* = 7.3 Hz, 1H), 7.26 – 7.19 (m, 3H), 7.17 – 7.09 (m, 1H), 7.11 – 6.96 (m, 2H), 5.90 (s, 1H), 3.58 (d, *J* = 13.8 Hz, 1H), 3.44 (s, 3H), 3.22 (m, 1H), 3.17 (d, *J* = 13.8 Hz, 1H), 3.06-2.89 (m, 2H), 2.86 (s, 3H), 2.54 (m, 4H), 2.39 (m, 1H), 2.05 (m, 2H), 1.54 (m, 2H), 1.40 (m, 3H), 1.10 (m, 2H); ¹³C NMR (125 MHz, CDCl₃) δ 129.2, 128.9, 127.8, 126.9, 121.5, 120.5, 119.7, 118.0, 52.8, 52.4, 51.3, 49.6, 47.3, 44.8, 38.9, 32.2, 27.2, 27.1, 27.1, 24.7, 24.5; HRMS (EI) calcd. for C₂₇H₃₇N₃O₂S[M]⁺, 467.2606. Found, 467.2601.

Scaffold Hopping

Taking the reported bioactive conformation of MI-2-2 and MIV-6R in the crystal structure (PDB code 4GQ4 and 4GO8) as the query, 3D-similarity search was performed using SHFATS^{67, 68}. SHFATS method combines the strength of molecular shape superposition and chemical feature matching for the 3D similarity calculation and ranking. Considering the drug-like properties of candidates, we built an in-house library comprising ~1600 compounds from existing drugs for 3D similarity searching. Before SHFATS calculation, diverse conformation generation for each molecule in the database was performed by Discovery Studio 2.5⁷². Subsequently, each conformer was aligned onto the query and calculated the 3D similarity score by SHFATS, the top-ranked molecules with SHFATS similarities >1.2 (maximum 2.0) were selected for further validation.

Molecular Docking

The molecular docking was performed by Glide program with Maestro v9.0 (Schrodinger, Inc.)^{69, 70}. The crystal structure of menin in complex with MIV-6R (PDB code 4GO8) was used as a target for the following molecular docking. Hydrogen atoms and charges of receptor were added using the "Protein Preparation Wizard" module in Maestro. To relieve steric clash, a partial minimization of the target was terminated when the root-mean-square deviation (rmsd) reached a maximum value of 0.3 Å. Amino acid residues within a distance of 14 Å around MIV-6R were defined as the binding site. For receptor grid generation, a scaling factor of 1.0 was set to van der Waals (VDW) radii of receptor atoms with the partial charge less than 0.25. Ligands were prepared by "LigPrep" module in Maestro, the generation of ionization states were carried out with Epik⁷⁸, a tools that are part of LigPrep. For ligand docking, extra-precision (XP) was adopted, at most 10 poses per ligand were written out, and the Glide scoring function (G-Score) was used to select the final poses for each ligand.

Menin Expression and Purification

The full-length of human menin were expressed and purified as described previously⁵⁴. For the further purification, a Q-Sepharose protocol (GE Healthcare) was performed after removing of the His6-SUMO tag.

Fluorescence polarization (FP) assays of inhibition of menin-MLL interaction

The fluorescence polarization reaction contains N-terminal FITC-labeled MLL₄₋₁₅ peptide (FITC-MBM1, ChinaPeptides Co., Ltd.)^{43, 45} at 30nM and menin at 600 nM in the FP buffer (50 mM HEPES, pH 7.5; 50 mM NaCl; 1mM DTT; 0.1mg/ml BSA). Compounds were added immediately after the mixture and incubated for 2 h in the darker at 4°C. Change in fluorescence polarization was monitored at 535 nm after excitations at 480 nm using the Envision protocol and applied to determine IC₅₀ values with the GraphPad Prism 5.0 program. Ki calculations were performed with the website *The Ki Calculator* website http://sw16.im.med.umich.edu/software/calc_ki/.

NMR spectroscopy

Both Carr-Purcell-Meiboom-Gill (CPMG) and saturation transfer difference (STD) experiments contained 5 μM menin in 50 mM phosphate buffer, pH7.5, dissolved in D₂O. Compounds in DMSO-D6 were added to a final concentration of 200 μM with 2-5% DMSO-D6. All NMR experiments were performed at 25 °C using 600 MHz BrukerAvance III spectrometer with a cryogenically cooled probe Brukerbiosp-in, Germany). Solvent-suppressed 1D ¹H CPMG (cpmgPr1d) were acquired using the pulse sequence [RD-90°-(τ-180°-τ)n-ACQ]. Water resonance was suppressed by presaturation using a 54.87 dB pulse during the recycle delay (RD) of 4s. The 90° pulse length was adjusted to about 11.82 μs. A total of 4 dummy scans and 64 free induction decays (FIDs) were collected into 64K acquisition points, covering a spectral width of 12 KHz (20ppm) and giving an acquisition time (ACQ) of 2.73s.

The STD experiment was acquired using the acquisition time of 1.71s, 4 dummy scans, and relaxation delay of 3s, followed by a 40 dB pulse with the irradiation frequency at 0.25 ppm or -1000 ppm alternatively. The total acquisition time was 31 minutes with 192 scans.

Stability Studies by DSF

Differential scanning fluorimetry were performed on a Quant Studio 6 Flex Real-Time PCR system (ABI). Each reaction were heated from 25 to 95 °C in 20 μL thermal shift buffer (50 mM Mops, pH6.48; 50 mM NaCl; 1 mM DTT) with 2.5μM menin, 5×SYPRO orange (Invitrogen) and a series of diluted compounds. All samples were tested in triplicate. ABsoluteqPCR Plate Seals (Thermo Scientific) were used to limit evaporation. Change of fluorescence signal of SYPRO orange was monitored and applied to determine the T_m of menin with Protein Thermal Shift Software Version 1.1 (ABI).

Surface Plasmon Resonance (SPR) Based Binding Assays

The SPR binding assays were performed on the Biacore T200 instrument (GE Healthcare) at 25 °C. Menin protein was covalently immobilized on a CM5 chip using a standard amine-coupling procedure in 10 mM sodium acetate (PH 5.0). The chip was first equilibrated with HBS-EP buffer (10mM HEPES

PH 7.4, 150mM NaCl, 3mM EDTA, 0.05% (v/v) surfactant P20, and 0.1% (v/v) DMSO) overnight. The compound was serially diluted with HBS-EP buffer and injected for 120s (contact phase), followed by 120s dissociation. KD values of the compound to menin were determined by Biacore T200 evaluation software (GE Healthcare).

Cell Viability Assays

MV4;11, KOPN-8, HL60 and Jurkat cells were cultured in RPMI-1640 medium supplemented with 10% FBS and 1% penicillin/streptomycin (Invitrogen). For the 7-d proliferation assay, plating densities were determined for each cell line on the basis of linear log-phase growth. Cells were counted and split back to the original plating density in fresh medium with compound resupplied on days 4. An AlamarBlue cell viability assay kit (Invitrogen) was employed. Plates were read for fluorescence intensity at 590 nm after excitations at 544 nm using the PHERAstar BMG microplate reader.

Inhibitor effects on cell cycle of MV4;11 leukemia cells

5×10⁵ mL⁻¹ MV4;11 cell were plated in 12-well plates and treated with compounds or 0.2% DMSO and incubated for 48h at 37°C in a 5% CO₂ incubator. Cells were harvested, washed with PBS buffer, and resuspended in cooled PBS buffer containing 70% ethanol. After fixation at 4°C for 24 h, samples were washed and resuspended in FACS buffer, and then incubated with RNase and propidium iodide (BD Pharmingen) at room temperature for 30min before flow cytometry.

Expression of CD11b

MV4;11 and KOPN-8 cells were plated in 12-well plates at an initial concentration of 3×10⁵ cells mL⁻¹ and treated with compounds or DMSO. At day three, cells were replanted with cell concentration adjusted to 3×10⁵ cells mL⁻¹ and compounds resupplied. After 7 days, cells were harvested, washed and resuspended with PBS Buffer with 1% BSA. PE mouse anti-human CD11b Ab (BD Pharmingen) were added and incubated at 4 °C for 30min before being analyzed by flow cytometry.

Cytospin/Wright-Giemsa staining

MV4;11 and KOPN-8 cells were plated in 12-well plates at an initial concentration of 3×10⁵ cells mL⁻¹ and treated with compounds or DMSO. Cells were counted and split back to the original plating density in fresh medium with compound resupplied every three-four days. Cells were harvested and centrifuged at 500rpm for 5min in Shandon cytospin3 (Thermo Scientific Cytospin) after 10 days of treatment. The slides were air-dried before staining with Wright-Giemsa stain (Baso).

Co-immunoprecipitation

HEK293 cells were plated and transfected with Flag-MLL_N plasmid using PEI (Sigma-Aldrich). After transfection, cells were treated with compounds or DMSO for 12h. Whole cell lysates were prepared by cell lysis buffer (Cell Signaling Technology) containing Protease Inhibitor Cocktail Roche) and compounds. Samples were centrifuged and

immunoprecipitated with ANTI-FLAG M-2 Magnetic beads (Sigma-Aldrich) at 4 °C for 2h. The immunoprecipitation samples were applied to SDS-PAGE electrophoresis and Western blotting after extensive PBS washing. Antibodies used include rabbit anti-menin (Cell Signaling Technology, Cat.6891), rabbit DYDDK tag antibody (Cell Signaling Technology, Cat.2368).

Real-Time PCR

Total RNA was extracted from cells using the Trizol Reagent kit (Invitrogen), and was then reverse transcribed using RevertAid First Strand cDNA Synthesis Kit (Thermo Scientific). Real-time PCR was performed with the SYBR Green Realtime PCR Master Mix (TOYOBO) and ran on the Quant Studio 6 Flex Real-Time PCR system (ABI). Relative quantification of genes transcript was carried out using the comparative C_t method.

AUTHOR INFORMATION

Corresponding Author

*Yaxi Yang, telephone 86-21-50806600-3508, email: yangyaxi@simm.ac.cn.

*Yuanyuan Zhang, telephone 86-21-50806600-5307, email: 10110700070@fudan.edu.cn.

* Cheng Luo, telephone: 86-21-50806600, email: cluo@simm.ac.cn.

Present Addresses

Shanghai Institute of Materia Medica, Chinese Academy of Sciences, Shanghai 201203, China

Author Contributions

Liyan Yue,^{†a,b} Juanjuan Du,^{†c} and Fei Ye,^{†d} contributed equally to this work.

Notes

The authors declare no competing financial interests.

Acknowledgements

This work was supported by the National Basic Research Program (2015CB910304), Hi-Tech Research and Development Program of China (2014AA01A302), the National Natural Science Foundation of China (21210003, 81430084, 81202398, 81402849 and 21272246), Zhejiang Province Natural Science Foundation (LQ14H300003), Public Projects of Zhejiang Province (2015C33159), Zhejiang Provincial Top Key Discipline of Biology and CAS Strategic Priority Research Program (XDA12020333)

References

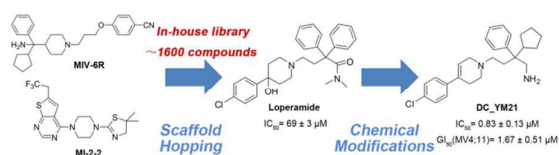
1. G. Egger, G. N. Liang, A. Aparicio and P. A. Jones, *Nature*, 2004, **429**, 457-463.

2. P. A. Jones and S. B. Baylin, *Cell*, 2007, **128**, 683-692.
3. M. A. Dawson and T. Kouzarides, *Cell*, 2012, **150**, 12-27.
4. H. Shen and P. W. Laird, *Cell*, 2013, **153**, 38-55.
5. L. Ho and G. R. Crabtree, *Nature*, 2010, **463**, 474-484.
6. R. A. Copeland, *ACS Med Chem Lett*, 2016, **7**, 124-127.
7. S. Heerboth, K. Lapinska, N. Snyder, M. Leary, S. Rollinson and S. Sarkar, *Genet Epigenet*, 2014, **6**, 9-19.
8. C. H. Arrowsmith, C. Bountra, P. V. Fish, K. Lee and M. Schapira, *Nat Rev Drug Discov*, 2012, **11**, 384-400.
9. J. Kaiser, *Science*, 2010, **330**, 576-578.
10. R. M. Campbell and P. J. Tummino, *J Clin Invest*, 2014, **124**, 64-69.
11. A. Erdmann, L. Halby, J. Fahy and P. B. Arimondo, *J Med Chem*, 2015, **58**, 2569-2583.
12. S. Chen, Y. Wang, W. Zhou, S. Li, J. Peng, Z. Shi, J. Hu, Y. C. Liu, H. Ding, Y. Lin, L. Li, S. Cheng, J. Liu, T. Lu, H. Jiang, B. Liu, M. Zheng and C. Luo, *J Med Chem*, 2014, **57**, 9028-9041.
13. X. Kong, L. Chen, L. Jiao, X. Jiang, F. Lian, J. Lu, K. Zhu, D. Du, J. Liu, H. Ding, N. Zhang, J. Shen, M. Zheng, K. Chen, X. Liu, H. Jiang and C. Luo, *J Med Chem*, 2014, **57**, 9512-9521.
14. F. Meng, S. Cheng, H. Ding, S. Liu, Y. Liu, K. Zhu, S. Chen, J. Lu, Y. Xie, L. Li, R. Liu, Z. Shi, Y. Zhou, Y. C. Liu, M. Zheng, H. Jiang, W. Lu, H. Liu and C. Luo, *J Med Chem*, 2015, **58**, 8166-8181.
15. K. K. Li, C. Luo, D. Wang, H. Jiang and Y. G. Zheng, *Med Res Rev* 2012, **32**, 815-867.
16. Y. Xie, R. Zhou, F. Lian, Y. Liu, L. Chen, Z. Shi, N. Zhang, M. Zheng, B. Shen, H. Jiang, Z. Liang and C. Luo, *Org Biomol Chem*, 2014, **12**, 9665-9673.
17. R. Zhou, Y. Xie, H. Hu, G. Hu, V. S. Patel, J. Zhang, K. Yu, Y. Huang, H. Jiang, Z. Liang, Y. G. Zheng and C. Luo, *J Chem Inf Model*, 2015, **55**, 2623-2632.
18. S. R. Bhaumik, E. Smith and A. Shilatifard, *Nat Struct Mol Biol* 2007, **14**, 1008-1016.
19. C. Martin and Y. Zhang, *Nat Rev Mol Cell Biol*, 2005, **6**, 838-849.
20. J. A. Latham and S. Y. R. Dent, *Nat Struct Mol Biol* 2007, **14**, 1017-1024.
21. R. A. Varier and H. T. Timmers, *Biochim. Biophys. Acta*, 2011, **1815**, 75-89.
22. M. Dalvai and K. Bystricky, *J Mammary Gland Biol Neoplasia*, 2010, **15**, 19-33.
23. C. Sawan and Z. Herceg, *Adv Genet*, 2010, **70**, 57-85.
24. A. J. Bannister and T. Kouzarides, *Cell Res*, 2011, **21**, 381-395.
25. M. Trissa, *Proc Natl Acad Sci*, 2001, **98**, 12902-12907.
26. H. Liu, E. H. Y. Cheng and J. J. D. Hsieh, *Biol Ther*, 2014, **8**, 1204-1211.
27. Y. Dou, T. A. Milne, A. J. Ruthenburg, S. Lee, J. W. Lee, G. L. Verdine, C. D. Allis and R. G. Roeder, *Nat Struct Mol Biol*, 2006, **13**, 713-719.
28. T. Senter, R. D. Gogliotti, C. Han, C. W. Locuson, R. Morrison, J. S. Daniels, T. Cierpicki, J. Grembecka, C. W. Lindsley and S. R. Stauffer, *Bioorg Med Chem Lett*, 2015, **25**, 2720-2725.
29. A. G. Muntean and J. L. Hess, *Annu Rev Pathol*, 2012, **7**, 283-301.

30. B. B. Zeisig, T. Milne, M. P. Garcia-Cuellar, S. Schreiner, M. E. Martin, U. Fuchs, A. Borkhardt, S. K. Chanda, J. Walker, R. Soden, J. L. Hess and R. K. Slany, *Mol Cell Biol*, 2003, **24**, 617-628.
31. T. A. Milne, Y. Dou, M. E. Martin, H. W. Brock, R. G. Roeder and J. L. Hess, *Proc Natl Acad Sci U S A*, 2005, **102**, 14765-14770.
32. C. Meyer, E. Kowarz, J. Hofmann, A. Renneville, J. Zuna, J. Trka, R. Ben Abdelali, E. Macintyre, E. De Braekeleer, M. De Braekeleer, E. Delabesse, M. P. de Oliveira, H. Cave, E. Clappier, J. J. van Dongen, B. V. Balgobind, M. M. van den Heuvel-Eibrink, H. B. Beverloo, R. Panzer-Grumayer, A. Teigler-Schlegel, J. Harbott, E. Kjeldsen, S. Schnittger, U. Koehl, B. Gruhn, O. Heidenreich, L. C. Chan, S. F. Yip, M. Krzywinski, C. Eckert, A. Moricke, M. Schrappe, C. N. Alonso, B. W. Schafer, J. Krauter, D. A. Lee, U. Zur Stadt, G. Te Kronnie, R. Sutton, S. Izraeli, L. Trakhtenbrot, L. Lo Nigro, G. Tsauro, L. Fechina, T. Szczepanski, S. Strehl, D. Ilencikova, M. Molkentin, T. Burmeister, T. Dingermann, T. Klingebiel and R. Marschalek, *Leukemia*, 2009, **23**, 1490-1499.
33. A. Forster, R. Pannell, L. F. Drynan, M. McCormack, E. C. Collins, A. Daser and T. H. Rabbitts, *Cancer Cell*, 2003, **3**, 449-458.
34. J. Wang, H. Iwasaki, A. Krivtsov, P. G. Febbo, A. R. Thorner, P. Ernst, E. Anastasiadou, J. L. Kutok, S. C. Kogan, S. S. Zinkel, J. K. Fisher, J. L. Hess, T. R. Golub, S. A. Armstrong, K. Akashi and S. J. Korsmeyer, *The EMBO Journal*, 2005, **24**, 368-381.
35. A. V. Krivtsov, Z. Feng, M. E. Lemieux, J. Faber, S. Vempati, A. U. Sinha, X. Xia, J. Jesneck, A. P. Bracken, L. B. Silverman, J. L. Kutok, A. L. Kung and S. A. Armstrong, *Cancer cell*, 2008, **14**, 355-368.
36. S. C. Chandrasekharappa, S. C. Guru, P. Manickam, S.-E. Olufemi, F. S. Collins, M. R. Emmert-Buck, L. V. Debelenko, Z. Zhuang, I. A. Lubensky, L. A. Liotta, J. S. Crabtree, Y. Wang, B. A. Roe, J. Weisemann, M. S. Boguski, S. K. Agarwal, M. B. Kester, Y. S. Kim, C. Heppner, Q. Dong, A. M. Spiegel, A. L. Burns and S. J. Marx, *Science*, 1997, **276**, 404-407.
37. S. J. Marx, *Nat Rev Cancer*, 2005, **5**, 367-375.
38. A. Yokoyama and M. L. Cleary, *Cancer Cell*, 2008, **14**, 36-46.
39. J. Huang, B. Gurung, B. Wan, S. Matkar, N. A. Veniaminova, K. Wan, J. L. Merchant, X. Hua and M. Lei, *Nature*, 2012, **482**, 542-546.
40. A. Yokoyama, Z. Wang, J. Wysocka, M. Sanyal, D. J. Aufiero, I. Kitabayashi, W. Herr and M. L. Cleary, *Mol Cell Biol*, 2004, **24**, 5639-5649.
41. K. Balogh, K. Rác, A. Patócs and L. Hunyady, *Trends in Endocrin Met* 2006, **17**, 357-364.
42. A. Yokoyama, T. C. Somerville, K. S. Smith, O. Rozenblatt-Rosen, M. Meyerson and M. L. Cleary, *Cell*, 2005, **123**, 207-218.
43. J. Grembecka, S. He, A. Shi, T. Purohit, A. G. Muntean, R. J. Sorenson, H. D. Showalter, M. J. Murai, A. M. Belcher, T. Hartley, J. L. Hess and T. Cierpicki, *Nat Chem Biol*, 2012, **8**, 277-284.
44. A. Shi, M. J. Murai, S. He, G. Lund, T. Hartley, T. Purohit, G. Reddy, M. Chruszcz, J. Grembecka and T. Cierpicki, *Blood*, 2012, **120**, 4461-4469.
45. J. Grembecka, A. M. Belcher, T. Hartley and T. Cierpicki, *J Biol Chem*, 2010, **285**, 40690-40698.
46. C. Caslini, Z. Yang, M. El-Osta, T. A. Milne, R. K. Slany and J. L. Hess, *Cancer Res*, 2007, **67**, 7275-7283.
47. T. Cierpicki and J. Grembecka, *Future Med Chem*, 2014, **6**, 447-462.
48. D. Borkin, S. H. He, H. Z. Miao, K. Kempinska, J. Pollock, J. Chase, T. Purohit, B. Malik, T. Zhao, J. Y. Wang, B. Wen, H. L. Zong, M. Jones, G. Danet-Desnoyers, M. L. Guzman, M. Talpaz, D. L. Bixby, D. X. Sun, J. L. Hess, A. G. Muntean, I. Maillard, T. Cierpicki and J. Grembecka, *Cancer Cell*, 2015, **27**, 589-602.
49. B. E. Li, T. Gan, M. Meyerson, T. H. Rabbitts and P. Ernst, *Blood*, 2013, **122**, 2039-2046.
50. S. He, B. Malik, D. Borkin, H. Miao, S. Shukla, K. Kempinska, T. Purohit, J. Wang, L. Chen, B. Parkin, S. N. Malek, G. Danet-Desnoyers, A. G. Muntean, T. Cierpicki and J. Grembecka, *Leukemia*, 2016, **30**, 508-513.
51. J. Pollock, D. Borkin, G. Lund, T. Purohit, E. Dyguda-Kazimierowicz, J. Grembecka and T. Cierpicki, *J Med Chem*, 2015, **58**, 7465-7474.
52. D. Borkin, J. Pollock, K. Kempinska, T. Purohit, X. Li, B. Wen, T. Zhao, H. Miao, S. Shukla, M. He, D. Sun, T. Cierpicki and J. Grembecka, *J Med Chem*, 2016, **59**, 892-913.
53. S. He, T. J. Senter, J. Pollock, C. Han, S. K. Upadhyay, T. Purohit, R. D. Gogliotti, C. W. Lindsley, T. Cierpicki, S. R. Stauffer and J. Grembecka, *J Med Chem*, 2014, **57**, 1543-1556.
54. L. Li, R. Zhou, H. Geng, L. Yue, F. Ye, Y. Xie, J. Liu, X. Kong, H. Jiang, J. Huang and C. Luo, *Bioorg Med Chem Lett*, 2014, **24**, 2090-2093.
55. H. Zhou, L. Liu, J. Huang, D. Bernard, H. Karatas, A. Navarro, M. Lei and S. Wang, *J Med Chem*, 2013, **56**, 1113-1123.
56. J. L. Medina-Franco, O. Mendez-Lucio, A. Duenas-Gonzalez and J. Yoo, *Drug Discov Today*, 2015, **20**, 569-577.
57. R. Ragno, S. Simeoni, S. Castellano, C. Vicidomini, A. Mai, A. Caroli, A. Tramontano, C. Bonaccini, P. Trojer, I. Bauer, G. Brosch and G. Sbardella, *J Med Chem*, 2007, **50**, 1241-1253.
58. G.-B. Li, L.-L. Yang, Y. Yuan, J. Zou, Y. Cao, S.-Y. Yang, R. Xiang and M. Xiang, *Methods*, 2015, **71**, 158-166.
59. J. Wang, L. Chen, S. H. Sinha, Z. Liang, H. Chai, S. Muniyan, Y.-W. Chou, C. Yang, L. Yan, Y. Feng, K. K. Li, M.-F. Lin, H. Jiang, Y. G. Zheng and C. Luo, *J Med Chem*, 2012, **55**, 7978-7987.
60. L. R. Vidler, P. Filippakopoulos, O. Fedorov, S. Picaud, S. Martin, M. Tomsett, H. Woodward, N. Brown, S. Knapp and S. Hoelder, *J Med Chem*, 2013, **56**, 8073-8088.
61. T. Sundarapandian, J. Shalini, S. Sugunadevi and L. K. Woo, *J Mol Graph Model*, 2010, **29**, 382-395.

62. H. Ratni, M. Rogers-Evans, C. Bissantz, C. Grundschober, J. L. Moreau, F. Schuler, H. Fischer, R. Alvarez Sanchez and P. Schnider, *J Med Chem*, 2015, **58**, 2275-2289.
63. M. J. Vainio, T. Kogej, F. Raubacher and J. Sadowski, *J Chem Inf Model*, 2013, **53**, 1825-1835.
64. G. A. Maggiora and M. A. Johnson, *John Wiley: New York*, 1990.
65. W. Zhou, X. Liu, Z. Tu, L. Zhang, X. Ku, F. Bai, Z. Zhao, Y. Xu, K. Ding and H. Li, *J Med Chem*, 2013, **56**, 7821-7837.
66. J. Wang, C. Luo, C. Shan, Q. You, J. Lu, S. Elf, Y. Zhou, Y. Wen, J. L. Vinkenborg, J. Fan, H. Kang, R. Lin, D. Han, Y. Xie, J. Karpus, S. Chen, S. Ouyang, C. Luan, N. Zhang, H. Ding, M. Merckx, H. Liu, J. Chen, H. Jiang and C. He, *Nat Chem*, 2015, **7**, 968-979.
67. X. Liu, H. Jiang and H. Li, *J Chem Inf Model*, 2011, **51**, 2372-2385.
68. W. Lu, X. Liu, X. Cao, M. Xue, K. Liu, Z. Zhao, X. Shen, H. Jiang, Y. Xu, J. Huang and H. Li, *J Med Chem*, 2011, **54**, 3564-3574.
69. T. A. Halgren, R. B. Murphy, R. A. Friesner, H. S. Beard, L. L. Frye, W. T. Pollard and J. L. Banks, *J Med Chem*, 2004, **47**, 1750-1759.
70. R. A. Friesner, J. L. Banks, R. B. Murphy, T. A. Halgren, J. J. Klicic, D. T. Mainz, M. P. Repasky, E. H. Knoll, M. Shelley, J. K. Perry, D. E. Shaw, P. Francis and P. S. Shenkin, *J Med Chem*, 2004, **47**, 1739-1749.
71. R. A. Laskowski and M. B. Swindells, *J Chem Inf Model*, 2011, **51**, 2778-2786.
72. A. Subasranjan, S. C and R. Hemant, *Drug Test Anal*, 2010, **2**, 107-112.
73. T. Iwamura, N. Hatae, T. Nagayama, H. Esaki, F. Kujime, M. Minami, M. Ishikura, T. Choshi, S. Hirano, C. Okada, E. Toyota and H. Nagasawa, *Heterocycles*, 2014, **88**, 663.
74. H. Xiong, T. A. Brugel, M. Balestra, D. G. Brown, K. A. Brush, C. Hightower, L. Hinkley, V. Hoesch, J. Kang, G. M. Koether, J. P. McCauley Jr, F. M. McLaren, L. M. Panko, T. R. Simpson, R. W. Smith, J. M. Woods, B. Brockel, V. Chhajlani, R. A. Gadiant, N. Spear, L. A. Sygowski, M. Zhang, J. Arora, N. Breyse, J. M. Wilson, M. Isaac, A. Slassi and M. M. King, *Bioorg Med Chem Lett*, 2010, **20**, 7381-7384.
75. R. A. Stokbroekx, J. Vandenberk, A. H. M. T. Van Heertum, G. M. L. W. Van Laar, M. J. M. C. Van der Aa, W. F. M. Van Bever and P. A. J. Janssen, *J Med Chem*, 1973, **16**, 782-786.
76. H. P. Ng, K. May, J. G. Bauman, A. Ghannam, I. Islam, M. Liang, R. Horuk, J. Hesselgesser, R. M. Snider, H. D. Perez and M. M. Morrissey, *J Med Chem*, 1999, **42**, 4680-4694.
77. R. Malik, A. P. Khan, I. A. Asangani, M. Cieslik, J. R. Prensner, X. Wang, M. K. Iyer, X. Jiang, D. Borkin, J. Escara-Wilke, R. Stender, Y. M. Wu, Y. S. Niknafs, X. Jing, Y. Qiao, N. Palanisamy, L. P. Kunju, P. M. Krishnamurthy, A. K. Yocum, D. Mellacheruvu, A. I. Nesvizhskii, X. Cao, S. M. Dhanasekaran, F. Y. Feng, J. Grembecka, T. Cierpicki and A. M. Chinnaiyan, *Nat Med*, 2015, **21**, 344-352.
78. J. C. Shelley, A. Cholleti, L. L. Frye, J. R. Greenwood, M. R. Timlin and M. Uchimaya, *J Comput Aid Mol Des*, 2007, **21**, 681-691.

Graphical abstract



Scaffold hopping combines with biochemical studies and medicinal chemistry optimizations, leading to potent inhibitors for menin-MLL interaction.